ScientificScholar®
Knowledge is power
Publisher of Scientific Journals

https://arabjchem.org

Arabian Journal of Chemistry

Article in Press

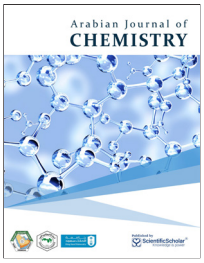

Original Article

Synthesis of new pyrazine-thiazole analogs: Molecular modeling, anticancer activity, and pharmacokinetic properties

Khadra B. Alomari[a], Hind A. Siddiq[a], Jihan Qurban[b], Abdulmajeed F. Alrefaei[c], Abrar Bayazeed[b], Nawaa Ali H. Alshammari[d], Hanadi A. Katouah[b], Nashwa M. El-Metwaly[b,e,*]

[a]Department of Physical Sciences, Chemistry Division, College of Science, Jazan University, P.O. Box. 114, Jazan 45142, Saudi Arabia
[b]Department of Chemistry, Faculty of Science, Umm Al Qura University, Makkah 24230, Saudi Arabia
[c]Department of Biology/Genetic and Molecular Biology Central Laboratory (GMCL), Jamoum University College, Umm Al-Qura University, Makkah 2203, Saudi Arabia
[d]Department of Chemistry, College of Science, Northern Border University, Arar 73222, Saudi Arabia
[e]Department of Chemistry, Faculty of Science, Mansoura University, Mansoura, Egypt

ARTICLE INFO

Keywords:
Carbonic anhydrase
Cytotoxic activity
DFT studies
Pharmacokinetic
Pyrazine-thiazole
Pyrazine-thiosemicarbazone

ABSTRACT

A series of pyrazine-linked thiazoles through amino-benzylidene bridges (**3**, **4**, **6**, **8**, **9**, and **11**) were synthesized, and their structures were confirmed through infrared (IR), nuclear magnetic resonance (NMR), and mass spectrometry (MS) analyses. The preparation strategy was built on the interaction between the thiosemicarbazone derived from 2-(4-acetylphenyl)amino-pyrazine (**1**) and several halo-carbonyl reagents. The density functional theory (DFT) studies of representative examples of the synthesized conjugates **4c**, **6c,** and **11c** revealed that they have non-planar configurations and different electronic properties, such as frontier molecular orbitals (FMOs) energies, polarizability, and hyperpolarizability. Moreover, the cytotoxic effectiveness of the synthesized pyrazine-thiazole analogs was appraised towards three tumor cell lines (Panc-1, HepG2, and MCF-7) and a normal cell line (WI-38), where it revealed good anti-tumor activity, likened to the standard drug erlotinib. Analog **6c** had a comparable inhibitory activity towards all tumor cell lines, especially against MCF-7 (IC_{50} = 5.51±0.09 µM), while analog **9** had significant cytotoxicity against Panc-1. Also, analog **11c** had strong activity, especially against HepG2 (IC_{50} = 8.01±0.35 µM). Moreover, the hybrids' ability to constrain human carbonic anhydrase isoforms was evaluated and exhibited strong inhibitory effects, comparable to acetazolamide (AZA), especially against Zinc containing metalloprotein catalyzes the reversible hydration of carbon dioxide (CAIX). The analog 3, which contains a thiazol-4-one moiety, displayed preferential efficiency against CAXII over CAIX, whereas hybrid **4c** had uniform inhibition toward both isoforms (IC50 = 0.052 ± 0.014 and 0.091 ± 0.018 µM, respectively). Further, the molecular dockage performance of the synthesized derivatives was conducted towards the 6CB0 amino **acid to** evaluate their binding affinities, interactions, and potential efficacy. Analogs **4b** and **6b** demonstrated high binding affinities along with multiple stabilizing interactions. Additionally, the pharmacokinetic properties of produced conjugates were explored using SwissADME. Hybrids 2, 3, and 4a-c exhibited high GI absorption and moderate solubility. Conversely, certain analogs like **11a-c** displayed low solubility and absorption. Finally, hybrid 6c exhibited strong anti-cancer activity against MCF-7 and noteworthy CA isoform inhibition comparable to AZA. Molecular docking studies revealed high binding affinities and pharmacokinetic analysis suggested fortunate absorption for some hybrids.

1. Introduction

Mammalian breast malignancy is highly lethal among females and, together with other forms of cancer, remains an important concern of global health [1-3]. Chemotherapy advancements are limited by issues such as efficacy, side effects, and drug resistance [4]. There is, therefore, a need for new drugs that provide higher levels of safety and specificity to the cancerous cells [5]. Consequently, drug discovery has focused on the advancement of new anti-tumor drugs to address the challenges being faced [6]. In this sense, carbonic anhydrase enzymes represent tumor-associated, cell-surface glycoproteins whose expression is induced under tumor hypoxia, especially some of its isoforms [7-9]. These enzymes thus play a critical role in enabling malignant tumor cells to adjust in the acid medium and are implicated in cancer progression through the catalytic transformation of carbon dioxide and water to bicarbonate and protons and through the non-catalytic roles of cellular signaling and tumor invasion [10-12]. However, heterocyclic compounds, particularly pyrazine and thiazole derivatives, have garnered considerable attention in medicinal chemistry owing to their versatile pharmaco-properties [13]. Pyrazines are aromatic heterocyclic compounds containing nitrogen that can originate from plants, animals, and marine sources [14-16]. Pyrazine ranks among the important classes of pharmacophores owing to the diverse nature of their pharmacological activity [17]. Due to the varied biological

***Corresponding author:**
E-mail address: nmmohamed@uqu.edu.sa; n_elmetwaly00@yahoo.com (N. El-Metwaly)

Received: 20 December, 2024 **Accepted:** 06 February, 2025 **Epub Ahead of Print:** 10 April 2025 **Published:** ***
DOI: 10.25259/AJC_300_2024

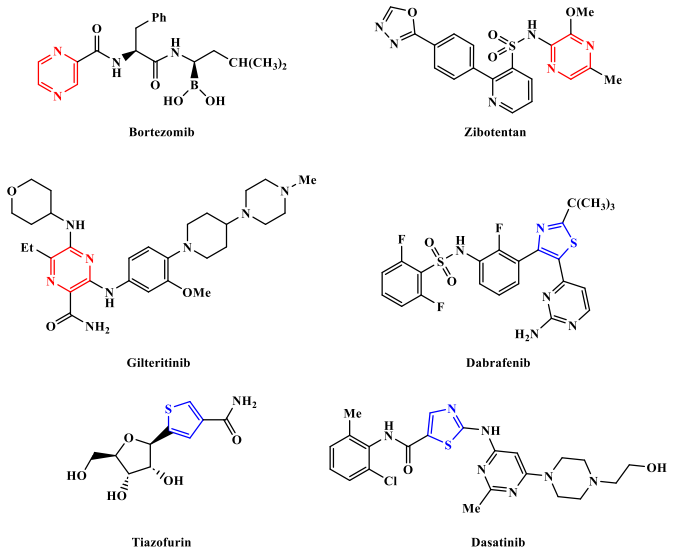

Figure 1. Pyrazine- and thiazole-based anti-cancer drugs.

activities of pyrazine-based drugs, various developments have occurred in the exploration of their synthetic pathways and anti-cancer activities (Figure 1) [18-20].

Meanwhile, thiazoles are another important class of nitrogen-containing heterocycles that are well-documented for their varied biological activities [21-23]. The heterocycles containing the thiazole moiety belong to a large family of therapeutic agents, which also include drugs such as antibiotics active against a wide range of tumors [24-27]. However, the synthetic thiazole derivatives have shown great promise in inhibiting cellular processes contributing to the progression of cancer and, therefore, are attractive candidates for developing drugs (Figure 1) [28-31]. The hybridization of pyrazine and thiazole scaffolds presents a synergistic strategy for developing potent anti-cancer agents [32-34]. Pyrazine-thiazole analogs demonstrate immense potential to interact with multiple molecular targets and hold advantages concerning multi-pathway inhibition, an essential strategy in fighting diseases like cancer. Considering the complimentary bioactivities between pyrazine and thiazole scaffolds, such hybrid compounds may potentially access a greater degree of selectivity and potency against cancerous cells than single scaffold drugs [35].

Building on our interest in the synthesis of novel pyrazine-thiazole analogs that potentially have pharmacological effectiveness, this work describes the synthetic pathway of some new hybrid heterocyclic compounds. It also evaluates their cytotoxic efficiency towards three tumor cell lines, inhibitory activities against carbonic anhydrases (CAIX and CAXII), and assesses their binding affinity through molecular docking with selected proteins. Additionally, their pharmacokinetic properties were investigated by means of SwissADME simulation predictions.

2. Materials and Methods

2.1. Materials and instruments

The solvents dioxane, tetrahydrofuran (THF), and acetic acid were selected based on their compatibility with the reaction components and their capacity to promote efficient reactions under mild conditions. Dioxane was used due to its superior solvating properties and its ability to stabilize intermediates during reactions, particularly those involving halogenated reagents. THF (as a polar aprotic solvent) was selected to enhance nucleophilic substitution or cyclization reactions while minimizing side products. Acetic acid was utilized for its dual functionality as both a solvent and a catalyst, especially in condensation reactions. Chloroacetic acid and phenacyl bromide were handled in a well ventilated fume hood, with researchers wearing appropriate personal protective equipment including gloves, goggles, and lab coats.

Melting points were assigned using the Gallenkamp-electric device. The infra-red spectra (KBr discs) were obtained from Thermo-Scientific Nicolet iS10 FTIR spectrophotometer. A JEOL spectrometer was employed to record the 1H- and 13C-Nuclear Magnetic Resonance (NMR) spectra at 500 MHz and 125 MHz, correspondingly, using DMSO-d6 as the solvent. A Quadrupole Gas Chromatography-Mass Spectra (GC-MS) (DSQII) instrument operating at 70 eV was utilized to acquire mass spectra. For elemental analysis of carbon, hydrogen, and nitrogen elements, a Perkin-Elmer 2400 analyzer was used.

2.2. 2-(1-(4-(Pyrazin-2-ylamino)phenyl)ethylidene)hydrazine-1-carbothioamide (2)

2-(4-Acetylphenyl)amino-pyrazine (1, 1.70 g, 8 mmol) and thiosemicarbazide (0.73 g, 8 mmol) were refluxed for three hrs in a solution of 35 mL ethanol and 1 mL acetic acid using a 100 mL round bottom flask (RBF). The resulting suspension was left to stand for a night, and a solid was precipitated. This solid was subsequently isolated, yielding the pyrazine-thiosemicarbazone compound **2.**

Yield = 1.86 g (81.3%), m.p. = 187-188°C. Retention factor **(R_f) = 0.44 (petroleum ether : AcOEt = 3:1).** IR (ν/cm^{-1}): 3340, 3228, 3196 (NH_2 and N-H), 1634 (C=N). ^{1}H NMR (δ/ppm): 2.36 (s, 3H, CH_3), 7.31 (d, J = 8.50 Hz, 2H), 7.67 (d, J = 8.50 Hz, 2H), 7.91 (s, 2H, NH_2), 8.47 (d, J = 2.00 Hz, 1H, pyrazine-H), 8.53 (d, J = 2.00 Hz, 1H, pyrazine-H), 8.61 (s, 1H, pyrazine-H), 9.26 (s, 1H, N-H), 11.34 (s, 1H, N-H). MS *m/z* (%): 286 (M^+, 17.03). Anal. Calcd. for $C_{13}H_{14}N_6S$ (286.10): C, 54.53; H, 4.93; N, 29.35%. Found: C, 54.67; H, 4.98; N, 29.26%.

2.3. 2-(2-(1-(4-(Pyrazin-2-ylamino)phenyl)ethylidene)hydrazineyl) thiazolin-4-one (3)

A mixture of pyrazine-thiosemicarbazone compound **2** (1.43 g, 5 mmol), chloroacetic acid (0.47 g, 5 mmol), and sodium acetate (0.50 g) in 25 mL acetic acid were heated with stirring for four hrs. The mixture was diluted with ice-water **(25 mL)** and the formed product was collected and crystallized from ethanol (30 mL) to yield the corresponding pyrazine-thiazolin-4-one analog 3 after cooling at 18-20°C for a duration of 12 hr.

Yield = 1.23 g (75.5%), m.p. = 231-232°C. **R_f = 0.38 (petroleum ether : AcOEt = 2:1).** IR (ν/cm^{-1}): 3332, 3225 (N-H), 1705 (C=O). ^{1}H NMR (δ/ppm): 2.35 (s, 3H, CH_3), 3.93 (s, 2H, CH_2), 7.27 (d, J = 8.50 Hz, 2H), 7.65 (d, J = 8.50 Hz, 2H), 8.45 (d, J = 2.00 Hz, 1H, pyrazine-H), 8.51 (d, J = 2.00 Hz, 1H, pyrazine-H), 8.60 (s, 1H, pyrazine-H), 9.33 (s, 1H, N-H), 11.76 (s, 1H, N-H). ^{13}C NMR (δ/ppm): 16.29, 36.17, 113.36 (2C), 128.74 (2C), 129.97, 135.08, 136.52, 142.65, 144.13, 147.88, 152.91, 163.56, 177.61. MS *m/z* (%): 326 (M^+, 67.11). Anal. Calcd. for $C_{15}H_{14}N_6OS$ (326.09): C, 55.20; H, 4.32; N, 25.75%. Found: C, 55.08; H, 4.37; N, 25.83%.

2.4. Synthesis of 5-arylidene-2-(2-(1-(4-(pyrazin-2-ylamino)phenyl) ethylidene)hydrazineyl)-thiazolin-4-one compounds 4a-c

A pyrazine-thiazolin-4-one hybrid **3** (0.65 g, 2 mmol) was combined with 30 mL of ethanoic acid in a 100 mL RBF. The resulting mixture was supplemented with 0.50 g of fused sodium ethanoate and 2 mmol of one of the following aldehydes: 4-methoxybenzaldehyde, 4-nitrobenzaldehyde, or 4-chlorobenzaldehyde. This solution underwent reflux for four hrs. Upon cooling to 20°C, a solid precipitate formed, which was subsequently isolated and crystallized using acetic acid (25 mL) after cooling at 20-22°C for a duration of 24 hrs. This process yielded the corresponding pyrazine-5-arylidine-thiazolin-4-ones, labeled as compounds **4a-c**.

5-(4-Methoxybenzylidene)-2-(2-(1-(4-(pyrazin-2-ylamino)phenyl) ethylidene)hydrazineyl)-thiazolin-4-one (***4a***):

Yield = 0.59 g (66.4%), m.p. = 284-285°C. **R_f = 0.40 (petroleum ether : AcOEt = 1:1).** IR (ν/cm^{-1}): 3312, 3147 (N-H), 1678 (C=O). ^{1}H NMR (δ/ppm): 2.36 (s, 3H, CH_3), 3.81 (s, 3H, OCH_3), 7.03 (d, J = 8.50 Hz, 2H), 7.30 (d, J = 8.50 Hz, 2H), 7.54 (d, J = 8.50 Hz, 2H), 7.67 (d, J = 8.50 Hz, 2H), 7.78 (s, 1H, C=CH), 8.46 (d, J = 2.00 Hz, 1H, pyrazine-H), 8.50 (d, J = 2.00 Hz, 1H, pyrazine-H), 8.58 (s, 1H,

pyrazine-H), 9.25 (s, 1H, N-H), 11.42 (s, 1H, N-H). ^{13}C NMR (δ/ppm): 16.24, 55.87, 113.30 (2C), 114.25 (2C), 127.11, 127.81, 128.68 (2C), 129.85, 130.38 (2C), 135.14, 136.55, 142.71, 144.22, 145.02, 147.76, 153.06, 163.41, 160.31, 169.32. MS *m/z* (%): 444 (M^+, 33.84). Anal. Calcd. for $C_{23}H_{20}N_6O_2S$ (444.14): C, 62.15; H, 4.54; N, 18.91%. Found: C, 62.33; H, 4.48; N, 18.78%.

5-(4-Nitrobenzylidene)-2-(2-(1-(4-(pyrazin-2-ylamino)phenyl) ethylidene)hydrazineyl)-thiazolin-4-one (***4b***):

Yield = 0.66 g (71.8%), m.p. > 310°C. **R_f = 0.58 (petroleum ether : AcOEt = 1:1).** IR (*ν*/cm^{-1}): 3335, 3194 (N-H), 1692 (C=O). ^{1}H NMR (δ/ppm): 2.37 (s, 3H, CH_3), 7.30 (d, *J* = 8.50 Hz, 2H), 7.69 (d, *J* = 8.50 Hz, 2H), 7.84 (d, *J* = 8.50 Hz, 2H), 7.92 (s, 1H, C=CH), 8.28 (d, *J* = 8.50 Hz, 2H), 8.48 (d, *J* = 2.00 Hz, 1H, pyrazine-H), 8.54 (d, *J* = 2.00 Hz, 1H, pyrazine-H), 8.63 (s, 1H, pyrazine-H), 9.46 (s, 1H, N-H), 11.58 (s, 1H, N-H). ^{13}C NMR (δ/ppm): 16.27, 113.46 (2C), 124.13 (2C), 128.02, 128.70 (2C), 129.34 (2C), 129.87, 135.05, 136.63, 140.71, 142.67, 144.18, 145.16, 147.26, 147.94, 152.85, 163.83, 171.10. MS *m/z* (%): 459 (M^+, 26.94). Anal. Calcd. for $C_{22}H_{17}N_7O_3S$ (459.11): C, 57.51; H, 3.73; N, 21.34%. Found: C, 57.31; H, 3.65; N, 21.20%.

5-(4-Chlorobenzylidene)-2-(2-(1-(4-(pyrazin-2-ylamino)phenyl) ethylidene)hydrazineyl)-thiazolin-4-one (***4c***):

Yield = 0.61 g (68.1%), m.p. = 297-298°C. **R_f = 0.47 (petroleum ether : AcOEt = 1:1).** IR (*ν*/cm^{-1}): 3309, 3165 (N-H), 1683 (C=O). ^{1}H NMR (δ/ppm): 2.35 (s, 3H, CH_3), 7.26 (d, *J* = 8.50 Hz, 2H), 7.50 (d, *J* = 8.50 Hz, 2H), 7.57 (d, *J* = 8.50 Hz, 2H), 7.70 (d, *J* = 8.50 Hz, 2H), 7.81 (s, 1H, C=CH), 8.48 (d, *J* = 2.00 Hz, 1H, pyrazine-H), 8.50 (d, *J* = 2.00 Hz, 1H, pyrazine-H), 8.58 (s, 1H, pyrazine-H), 9.34 (s, 1H, N-H), 11.47 (s, 1H, N-H). ^{13}C NMR (δ/ppm): 16.24, 113.33 (2C), 127.74, 128.56 (2C), 129.01 (2C), 129.38 (2C), 129.78, 133.04, 133.75, 135.21, 136.51, 142.63, 144.26, 145.08, 147.87, 152.90, 163.50, 168.66. MS *m/z* (%): 450 (M^+ + 2, 11.07), 448 (M^+, 32.91). Anal. Calcd. for $C_{22}H_{17}ClN_6OS$ (448.09): C, 58.86; H, 3.82; N, 18.72%. Found: C, 58.65; H, 3.71; N, 18.88%.

2.5. Synthesis of 4-aryl-2-(2-(1-(4-(pyrazin-2-ylamino)phenyl)ethylidene) hydrazineyl)-thiazole derivatives 6a-c

A pyrazine-thiosemicarbazone analog **2** (0.57 g, 2 mmol) was solubilized in 25 mL of dioxane within a 100 mL RBF. Subsequently, a phenacyl bromide derivative (2 mmol) - either *p*-methoxyphenacyl bromide, *p*-nitrophenacyl bromide, or *p*-chlorophenacyl bromide was introduced along with 0.2 mL of triethylamine. The mixture underwent reflux for four hrs, followed by cooling to 25°C to induce precipitation. The product was then filtered and crystallized from dioxane **(30 mL),** yielding the corresponding pyrazine-thiazole analogs **6a**, **6b**, and **6c**, after cooling at 20°C for a duration of 12 hrs.

4-(4-Methoxyphenyl)-2-(2-(1-(4-(pyrazin-2-ylamino)phenyl) ethylidene)hydrazineyl)-thiazole (***6a***):

Yield = 0.54 g (64.9%), m.p. = 266-267°C. **R_f = 0.46 (petroleum ether : AcOEt = 2:1).** IR (*ν*/cm^{-1}): 3331, 3213 (N-H), 1617 (C=N). ^{1}H NMR (δ/ppm): 2.63 (s, 3H, CH_3), 3.79 (s, 3H, OCH_3), 7.01 (d, *J* = 9.00 Hz, 2H), 7.14 (s, 1H, thiazole-H), 7.33 (d, *J* = 8.50 Hz, 2H), 7.56 (d, *J* = 9.00 Hz, 2H), 7.70 (d, *J* = 8.50 Hz, 2H), 8.41 (d, *J* = 2.00 Hz, 1H, pyrazine-H), 8.48 (d, *J* = 2.00 Hz, 1H, pyrazine-H), 8.61 (s, 1H, pyrazine-H), 9.08 (s, 1H, N-H), 11.74 (s, 1H, N-H). ^{13}C NMR (δ/ppm): 16.46, 55.88, 106.44, 113.76 (2C), 114.95 (2C), 126.28, 128.57 (4C), 129.70, 134.91, 136.04, 142.63, 143.38, 148.35, 152.53, 158.21, 160.40, 171.15. MS *m/z* (%): 416 (M^+, 42.35). Anal. Calcd. for $C_{22}H_{20}N_6OS$ (416.14): C, 63.44; H, 4.84; N, 20.18%. Found: C, 63.27; H, 4.75; N, 20.09%.

4-(4-Nitrophenyl)-2-(2-(1-(4-(pyrazin-2-ylamino)phenyl)ethylidene) hydrazineyl)-thiazole (***6b***):

Yield = 0.59 g (68.4%), m.p. = 289-290°C. **R_f = 0.61 (petroleum ether : AcOEt = 2:1).** IR (*ν*/cm^{-1}): 3334, 3221 (N-H), 1629 (C=N). ^{1}H NMR (δ/ppm): 2.67 (s, 3H, CH_3), 7.19 (s, 1H, thiazole-H), 7.35 (d, *J* = 8.50 Hz, 2H), 7.67 (d, *J* = 8.50 Hz, 2H), 7.96 (d, *J* = 8.50 Hz, 2H), 8.30 (d, *J* = 8.50 Hz, 2H), 8.48 (d, *J* = 2.00 Hz, 1H, pyrazine-H), 8.55 (d, *J* = 2.00 Hz, 1H, pyrazine-H), 8.64 (s, 1H, pyrazine-H), 9.13 (s, 1H, N-H), 11.83 (s, 1H, N-H). ^{13}C NMR (δ/ppm): 16.52, 107.13, 113.64 (2C), 124.88 (2C), 126.31 (2C), 128.70 (2C), 129.83, 134.87, 136.13, 138.92, 142.56, 143.48, 147.73, 148.26, 152.66, 158.35, 171.01. MS *m/z* (%): 431 (M^+, 34.77). Anal. Calcd. for $C_{21}H_{17}N_7O_2S$ (431.12): C, 58.46; H, 3.97; N, 22.72%. Found: C, 58.31; H, 3.88; N, 22.84%.

4-(4-Chlorophenyl)-2-(2-(1-(4-(pyrazin-2-ylamino)phenyl)ethylidene) hydrazineyl)-thiazole (***6c***):

Yield = 0.52 g (61.9%), m.p. = 274-275°C. **R_f = 0.52 (petroleum ether : AcOEt = 2:1).** IR (*ν*/cm^{-1}): 3327, 3210 (N-H), 1623 (C=N). ^{1}H NMR (δ/ppm): 2.65 (s, 3H, CH_3), 7.13 (s, 1H, thiazole-H), 7.28 (d, *J* = 8.50 Hz, 2H), 7.51 (d, *J* = 8.50 Hz, 2H), 7.67 (d, *J* = 8.50 Hz, 2H), 7.83 (d, *J* = 8.50 Hz, 2H), 8.46 (d, *J* = 2.00 Hz, 1H, pyrazine-H), 8.51 (d, *J* = 2.00 Hz, 1H, pyrazine-H), 8.60 (s, 1H, pyrazine-H), 9.10 (s, 1H, N-H), 11.73 (s, 1H, N-H). ^{13}C NMR (δ/ppm): 16.34, 106.61, 113.83 (2C), 128.65 (2C), 129.04 (2C), 129.57 (3C), 132.22, 134.10, 135.08, 136.17, 142.75, 143.40, 148.55, 152.45, 157.92, 171.06. MS *m/z* (%): 422 (M^+ + 2, 13.29), 420 (M^+, 40.78). Anal. Calcd. for $C_{21}H_{17}ClN_6S$ (420.09): C, 59.92; H, 4.07; N, 19.97%. Found: C, 60.08; H, 4.13; N, 20.08%.

2.6. Synthesis of pyrazine-thiazole compounds 8a, 8b, and 9

A solution of pyrazine-thiosemicarbazone compound **2** (0.57 g, 2 mmol) in 25 mL dioxane, chloroacetone, 3-chloroacetyl acetone, and/or ethyl 4-chloroacetoacetate (2 mmol) and 0.2 mL triethylamine were combined. The mixture was refluxed for 4 hrs and then chilled to 25°C. The obtained solid was filtered upon cooling to produce the conforming pyrazine-thiazole analogs **8a**, **8b**, and **9**.

4-Methyl-2-(2-(1-(4-(pyrazin-2-ylamino)phenyl)ethylidene)hydrazin-eyl)thiazole (***8a***):

Yield = 0.46 g (70.9%), m.p. = 246-247°C. **R_f = 0.28 (petroleum ether : AcOEt = 1:1).** IR (*ν*/cm^{-1}): 3337, 3205 (N-H), 1620 (C=N). ^{1}H NMR (δ/ppm): 2.17 (s, 3H, CH_3), 2.58 (s, 3H, CH_3), 6.26 (s, 1H, thiazole-H), 7.28 (d, *J* = 8.50 Hz, 2H), 7.71 (d, *J* = 8.50 Hz, 2H), 8.40 (d, *J* = 2.00 Hz, 1H, pyrazine-H), 8.46 (d, *J* = 2.00 Hz, 1H, pyrazine-H), 8.58 (s, 1H, pyrazine-H), 9.04 (s, 1H, N-H), 11.30 (s, 1H, N-H). ^{13}C NMR (δ/ppm): 16.32, 16.70, 104.62, 113.81 (2C), 128.68 (2C), 129.73, 134.57, 136.13, 142.45, 143.24, 147.10, 151.86, 160.06, 164.97. MS *m/z* (%): 324 (M^+, 28.48). Anal. Calcd. for $C_{16}H_{16}N_6S$ (324.12): C, 59.24; H, 4.97; N, 25.91%. Found: C, 59.35; H, 4.91; N, 25.85%.

5-Acetyl-4-methyl-2-(2-(1-(4-(pyrazin-2-ylamino)phenyl)ethylidene) hydrazineyl)thiazole ***(8b):***

Yield = 0.46 g (62.8%), m.p. = 256-257°C. **R_f = 0.41 (petroleum ether : AcOEt = 1:1).** IR (*ν*/cm^{-1}): 3343, 3227 (N-H), 1684 (C=O). ^{1}H NMR (δ/ppm): 2.45 (s, 3H, thiazole-CH_3), 2.54 (s, 3H, $COCH_3$), 2.62 (s, 3H, CH_3), 7.25 (d, *J* = 8.50 Hz, 2H), 7.68 (d, *J* = 8.50 Hz, 2H), 8.38 (d, *J* = 2.00 Hz, 1H, pyrazine-H), 8.47 (d, *J* = 2.00 Hz, 1H, pyrazine-H), 8.60 (s, 1H, pyrazine-H), 9.11 (s, 1H, N-H), 11.43 (s, 1H, N-H). ^{13}C NMR (δ/ppm): 16.36, 16.63, 27.94, 113.75 (2C), 127.42, 128.70 (2C), 129.81, 134.90, 135.88, 142.67, 143.31, 152.08, 155.64, 160.29, 163.55, 195.50. MS *m/z* (%): 366 (M^+, 31.55). Anal. Calcd. for $C_{18}H_{18}N_6OS$ (366.13): C, 59.00; H, 4.95; N, 22.93%. Found: C, 59.13; H, 4.98; N, 22.85%.

Ethyl 2-(2-(2-(1-(4-(pyrazin-2-ylamino)phenyl)ethylidene)hydrazineyl)-thiazol-4-yl)acetate (***9***):

Yield = 0.42 (53.0%(, m.p. = 228-229°C. **R_f = 0.48 (petroleum ether : AcOEt = 1:1).** IR (ν/cm^{-1}): 3318, 3192 (N-H), 1731 (C=O). ^{1}H NMR (δ/ppm): 1.26 (t, *J* = 7.00 Hz, 3H, O-CH_2-$\underline{CH_3}$), 2.35 (s, 3H, CH_3), 3.75 (s, 2H, -CH_2-COOEt), 4.16 (t, *J* = 7.00 Hz, 2H, O-$\underline{CH_2}$-CH_3), 6.43 (s, 1H, thiazole-H), 7.30 (d, *J* = 8.50 Hz, 2H), 7.72 (d, *J* = 8.50 Hz, 2H), 8.38 (d, *J* = 2.00 Hz, 1H, pyrazine-H), 8.45 (d, *J* = 2.00 Hz, 1H, pyrazine-H), 8.57 (s, 1H, pyrazine-H), 9.17 (s, 1H, N-H), 11.56 (s, 1H, N-H). ^{13}C NMR (δ/ppm): 14.31, 16.43, 35.24, 61.20, 104.09, 113.71 (2C), 128.65 (2C), 129.80, 135.02, 136.27, 142.50, 143.11, 145.56, 151.98, 159.92, 167.38, 169.13. MS *m/z* (%): 396 (M^+, 20.37). Anal. Calcd. for $C_{19}H_{20}N_6O_2S$ (396.14): C, 57.56; H, 5.08; N, 21.20%. Found: C, 57.38; H, 5.15; N, 21.27%.

2.7 Synthesis of 5-arylazo-4-methyl-2-(2-(1-(4-(pyrazin-2-ylamino) phenyl)ethylidene)-hydrazineyl)thiazole compounds 11a-c

A 100 mL RBF was occupied by a solution of the pyrazine-thiosemicarbazone analog **2** (0.57 g, 2 mmol) in 25 mL THF and 0.4 mL triethylamine. To this solution, the corresponding *N*-aryl-2-oxo-propanehydrazonoyl chloride **10a**, **10b**, and/or **10c** (2 mmol) was poured and then let to reflux for four hrs. Finally, the precipitate was collected and crystallized with ethanol **(35 mL)** to produce the corresponding pyrazine-thiazole analogs **11a**, **11b** and **11c**, after cooling at 25°C for a duration of 8 hrs.

5-((4-Methoxyphenyl)azo)-4-methyl-2-(2-(1-(4-(pyrazin-2-ylamino) phenyl)ethylidene)-hydrazineyl)thiazole ***(11a):***

Yield = 0.51 g (55.6%), m.p. = 217-218°C. **R_f = 0.36 (petroleum ether : AcOEt = 1:2).** IR (ν/cm^{-1}): 3308, 3226 (N-H), 1637 (C=N). ^{1}H NMR (δ/ppm): 2.42 (s, 3H, CH_3), 2.65 (s, 3H, CH_3), 3.81 (s, 3H, OCH_3), 7.01 (d, *J* = 9.00 Hz, 2H), 7.25 (d, *J* = 8.50 Hz, 2H), 7.67 (d, *J* = 8.50 Hz, 2H), 7.78 (d, *J* = 9.00 Hz, 2H), 8.38 (d, *J* = 2.00 Hz, 1H, pyrazine-H), 8.45 (d, *J* = 2.00 Hz, 1H, pyrazine-H), 8.61 (s, 1H, pyrazine-H), 9.16 (s, 1H, N-H), 11.13 (s, 1H, N-H). ^{13}C NMR (δ/ppm): 11.69, 16.33, 55.81, 113.84 (2C), 114.38 (2C), 128.08 (2C), 128.65 (2C), 129.87, 132.13, 134.16, 134.73, 136.27, 142.70, 143.55, 144.41, 152.21, 158.26, 160.92, 168.02. MS *m/z* (%): 458 (M^+, 19.83). Anal. Calcd. for $C_{23}H_{22}N_8OS$ (458.16): C, 60.25; H, 4.84; N, 24.44%. Found: C, 60.36; H, 4.80; N, 24.52%.

5-((4-Nitrophenyl)azo)-4-methyl-2-(2-(1-(4-(pyrazin-2-ylamino)phenyl)ethylidene)-hydrazineyl)thiazole ***(11b):***

Yield = 0.59 g (62.3%), m.p. = 252-253°C. **R_f = 0.54 (petroleum ether : AcOEt = 1:2).** IR (ν/cm^{-1}): 3321, 3233 (N-H), 1641 (C=N). ^{1}H NMR (δ/ppm): 2.43 (s, 3H, CH_3), 2.67 (s, 3H, CH_3), 7.28 (d, *J* = 8.50 Hz, 2H), 7.70 (d, *J* = 8.50 Hz, 2H), 7.86 (d, *J* = 8.50 Hz, 2H), 8.24 (d, *J* = 8.50 Hz, 2H), 8.43 (d, *J* = 2.00 Hz, 1H, pyrazine-H), 8.50 (d, *J* = 2.00 Hz, 1H, pyrazine-H), 8.63 (s, 1H, pyrazine-H), 9.18 (s, 1H, N-H), 11.22 (s, 1H, N-H). ^{13}C NMR (δ/ppm): 11.75, 16.60, 113.72 (2C), 124.15 (2C), 124.89 (2C), 128.81 (2C), 129.78, 132.94, 134.80, 136.32, 142.47, 143.63, 144.56, 145.96, 148.22, 152.51, 159.07, 168.18. MS *m/z* (%): 473 (M^+, 23.05). Anal. Calcd. for $C_{22}H_{19}N_9O_2S$ (473.14): C, 55.80; H, 4.04; N, 26.62%. Found: C, 55.64; H, 4.11; N, 26.50%.

5-((4-Chlorophenyl)azo)-4-methyl-2-(2-(1-(4-(pyrazin-2-ylamino) phenyl)ethylidene)-hydrazineyl)thiazole ***(11c):***

Yield = 0.53 g (57.3%), m.p. = 241-242°C. **R_f = 0.42 (petroleum ether : AcOEt = 1:2).** IR (ν/cm^{-1}): 3328, 3217 (N-H), 1634 (C=N). ^{1}H NMR (δ/ppm): 2.43 (s, 3H, CH_3), 2.65 (s, 3H, CH_3), 7.26 (d, *J* = 8.50 Hz, 2H), 7.38 (d, *J* = 8.50 Hz, 2H), 7.67 (d, *J* = 8.50 Hz, 2H), 7.75 (d, *J* = 8.50 Hz, 2H), 8.38 (d, *J* = 2.00 Hz, 1H, pyrazine-H), 8.46 (d, *J* = 2.00 Hz, 1H, pyrazine-H), 8.60 (s, 1H, pyrazine-H), 9.08 (s, 1H, N-H), 11.16 (s, 1H, N-H). ^{13}C NMR (δ/ppm): 11.66, 16.27, 113.85 (2C), 127.47 (2C), 128.71 (2C), 129.10 (2C), 129.75, 132.52, 134.50, 135.11, 136.25, 138.34, 142.56, 143.31, 144.14, 152.38, 158.05, 167.91. MS *m/z* (%): 462 (M^+, 15.26). Anal. Calcd. for $C_{22}H_{19}ClN_8S$ (462.11): C, 57.08; H, 4.14; N, 24.20%. Found: C, 56.90; H, 4.05; N, 24.10%.

2.8. DFT modeling

Utilizing the Becke's three-parameter exchange functional with the Lee-Yang-Parr correlation functional (B3LYP) and 6-311++G(d,p) basis set of the Gaussian 09W (version 9.5) [36-39], the derivatives were geometrically optimized, and their electronic and frontier molecular orbitals (FMOs) were analyzed via GaussView (version 6.0) [40]. The convergent criteria used was the default SCF convergence (10^8) with maximum displacement 1.8×10^{-3}. The DMol3 module of the Materials Studio's was used in Fukui indices [41] assessment at B3LYP/DNP 3.5 level [42].

2.9. Cytotoxic assay

A diverse assortment of cell lines, which encompass Panc-1, HepG2, MCF-7, along with WI-38, a representative normal cell line, was employed to conduct an *in vitro* anti-cancer assay aimed at evaluating the efficacy of the synthetic benzothiazole-thiadiazole hybrids, utilizing the well-established MTT assay methodology for accurate measurement of cell viability and proliferation [43]. The cells were cultured in RPMI-1640 medium supplemented with 10% fetal bovine serum (FBS). During the incubation phase at 37°C in a 5% CO_2 environment, antibiotics inclusive of 100 U/mL penicillin and 100 µg/mL streptomycin were introduced to the cells. In the next phase, the cells were seeded in a 96-well plate at a density of 1.0×10^4 cells/well, which was maintained at 37°C for 48 hrs in the same CO_2-enriched environment. Following this incubation period, the cells were subjected to varying concentrations of the compounds for 24 hrs. The serum was then ousted, and 150 µL of 10% w/v trichloroacetic acid was added in each well and the mixture was then incubated at 4°C for 1 hr. Once this step was complete, the cells were washed with TCA alongside water three times to reduce SRB protein binding. In the well, 70 µL of SRB was added alongside 0.4% of the compound, and this mixture was then incubated at room temperature for 10 mins. The bromide dye was removed alongside utilizing the 1% acetic acid compound. This mixture was left to dry out for 24 hrs, and finally, the wells were solubilized utilizing 50 µL of 10 mM tris base (pH 7.4) for 5 mins, while being shaken at 1600 rpm.

2.10. Carbonic anhydrase assay

The various compounds that were carefully synthesized in the laboratory were subsequently evaluated through a series of assays to determine their efficacy as inhibitors against four specific carbonic anhydrase isoforms that are physiologically significant, which include the trans-membrane tumor-associated isoforms *hCA IX* and *hCA XII*, alongside the targeted cytosolic isoforms *hCA IX* and *hCA XII*, and this evaluation was conducted utilizing the CO_2 hydrase methodology [44]. The carbonic anhydrase-mediated hydration of CO_2 described in this report was evaluated using an Applied Photo-physics stopped-flow instrument. The enzymes utilized are recombinant proteins synthesized in our laboratory. Phenol red was employed as an indicator at a concentration of 0.2 mM, operating at the absorbance peak of 557 nm, with a buffer solution of 20 mM Hepes (pH 7.5) and 20 mM Na_2SO_4 to maintain a consistent ionic strength. The initial rates of the CA-catalyzed CO_2 hydration reaction were monitored over 10 to 100 seconds, with CO_2 concentrations varying from 1.7 to 17 mM to ascertain the kinetic parameters and inhibition constants. For each inhibitor, a minimum of six traces corresponding to the initial 5-10% of the reaction were analyzed to determine the initial velocity. The rates of the uncatalyzed reactions were measured in a similar manner and subsequently subtracted from the total observed rates. Stock solutions of the inhibitor at 0.1 mM were prepared in distilled-deionized water, followed by dilutions down to 0.01 mM using the assay buffer. Prior to the assay, the inhibitor and enzyme solutions were preincubated together for 15 mins at room temperature to facilitate compound formation. The inhibition constants were calculated using non-linear

least-squares methods with PRISM 3 and the Cheng-Prusoff equation, representing the average from at least three separate determinations.

2.11. Molecular docking

The process of molecular docking was meticulously conducted employing the advanced software M.O.E.2019., which facilitated the exploration and analysis of the ligand structures corresponding to a variety of pyrazine-thiazole analogs, specifically the compounds numbered **2, 3, 4a-c**, **6a-c**, **8a, 8b**, **9**, and **11a-c**. In the selection process, the protein of interest was judiciously chosen in its .pdb format, which was derived from the intricately detailed co-crystalized structure of focal adhesion kinase (FAK), precisely represented by the entry identified as 6CB0 within the comprehensive Protein Data Bank [33]. FAK is a non-receptor tyrosine kinase that is essential in the processes of tumor progression, metastasis, and angiogenesis. Elevated levels of FAK have been detected in various cancer types, such as breast, pancreatic, and liver cancers, which are the focus of this study. Its participation in numerous signaling pathways that govern cell adhesion, migration, and survival positions it as a promising target for therapeutic intervention.

3. Results and Discussion

3.1. Synthesis of pyrazine-thiazole hybrids 3, 4, 6, 8, 9, and 11

The preparation of our pyrazine-based thiosemicarbazone precursor **2** has been achieved by condensation of 2-(4-acetylphenyl)amino-pyrazine (**1**) [45] with thiosemicarbazide in boiling ethanol and acetic acid **(1 mL).** The pyrazine-thiosemicarbazone derivative **2** undergoes a cyclization reaction involving its thioamide portion when combined with chloroacetic acid in boiling acetic acid containing sodium acetate, leading to the formation of the corresponding pyrazine-thiazolin-4-one compound **3** (Scheme 1). The thiazolin-4-one ring structure in compound 3 has a methylene group with sufficient reactivity toward Knoevenagel condensation with aromatic aldehydes (*p*-methoxy-, *p*-nitro-, and *p*-chlorobenzaldehyde). The reaction proceeds by heating in a mixture of acetic acid and sodium acetate, where the target compounds **4a-c**, 5-arylidene-2-(2-(1-(4-(pyrazin-2-ylamino)phenyl)ethylidene) hydrazineyl)-thiazolin-4-ones, were successfully synthesized. The molecular structures of pyrazine-thiazoles **3** and **4a-c** were determined through a comprehensive analysis of their IR, ^{1}H NMR, ^{13}C NMR, and MS data.

The absorption frequencies were correlated with the chemical environment of the carbonyl group in the synthesized pyrazine-thiazole analogs 3 and 4a-c. The cyclic carbonyl group in thiazolin-4-one compound 3 was observed at the expected absorption frequency of 1705 cm^{-1}. The suggested conjugation, as a result of the introduction of the arylidene system at the fifth position of thiazolin-4-one compounds 4a-c, lowers the frequency of the carbonyl group to 1678, 1692, and 1683 cm^{-1}, respectively. In addition, the nature of the substituent at the *para*-position of the benzylidene group affected the absorption frequency of the carbonyl group in compounds 4a-c. The electron-donating methoxy group in compound 4a promoted a sharp decrease in the carbonyl frequency to 1678 cm^{-1}. The electron-withdrawing nitro group in compound 4b somewhat compensated for the effect of conjugation; the carbonyl frequency was recorded at 1692 cm^{-1}.

The ^{1}H NMR spectrum of **4a** revealed distinct singlet signals for the protons of the methyl (N=C-CH_3) and methoxy (-OCH_3) groups at δ 2.36 and 3.81 ppm, individually. The doublet signals at δ 7.03, 7.30, 7.54, and 7.67 ppm were attributed to the phenylene group protons. A singlet at δ 7.78 ppm indicated the presence of the olefinic proton. The three protons of pyrazine-ring were assigned as two doublet (δ 8.46 and 8.50 ppm) and singlet (δ 8.58 ppm) signals. The singlet signals that were detected at δ 9.25 and 11.42 ppm indicated the protons of two N-H groups. When scanning chemical shift values for the olefinic proton in compounds 4a-c, it was found that they were directly influenced by the electronic nature of the substituted group at the benzylidene group. The olefinic proton in compound 4a was observed at a lower chemical shift of δ 7.78 ppm due to the presence of an electron-donating methoxy group. The electron-withdrawing nitro group in compound 4c promoted a de-shielding effect on the olefinic proton to a higher chemical shift of δ 7.92 ppm.

The cyclization reaction caused due to exposure of pyrazine-thiosemicarbazone 2 to chloroacetic acid involves several steps (Scheme 2). Initially, the thiol group undergoes alkylation with chloroacetic acid, resulting in the release of an HCl molecule and the formation of an intermediate (A). This intermediate then quickly undergoes cyclization, during which a water molecule is eliminated. The resulting intermediate (B) rapidly tautomerizes, ultimately producing the desired pyrazine-thiazolin-4-one hybrid 3.

Also, thiosemicarbazone 2 has been employed as a starting material for generating the second set of pyrazine-thiazole analogs **6a-c**. These analogs, characterized by an aryl substituent at the thiazole ring's fourth position, were synthesized through Hantzsch-type reactions. The process involved reacting compound **2** with various phenacyl bromides, specifically 4-methoxy-, 4-nitro-, and 4-chlorophenacyl bromide, as outlined in Scheme 3. The production of the third set of pyrazine-thiazole conjugates, **8a** and **8b**, featuring a methyl substituent at the fourth position of the newly formed thiazole ring, was achieved through a similar process that involved reacting the pyrazine-thiosemicarbazone **2** with either chloroacetone or 4-chloroacetylacetone in a mixture of

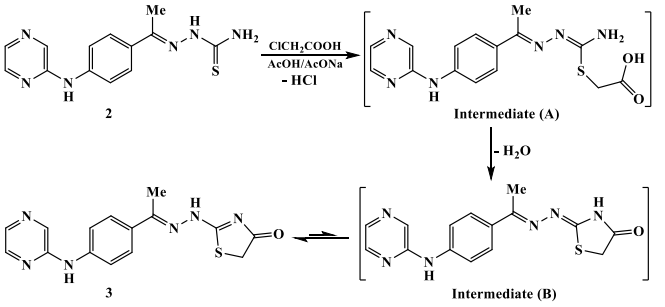

Scheme 2. The mechanism for cyclization of pyrazine-thiosemicarbazone 4 with chloroacetic acid.

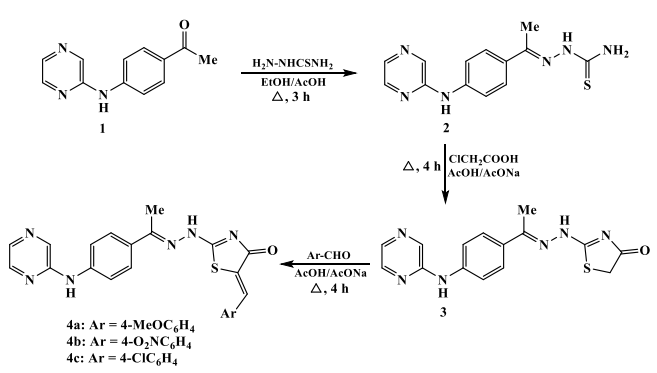

Scheme 1. Synthesis of pyrazine-thiazolin-4-one analogs 3 and 4a-c.

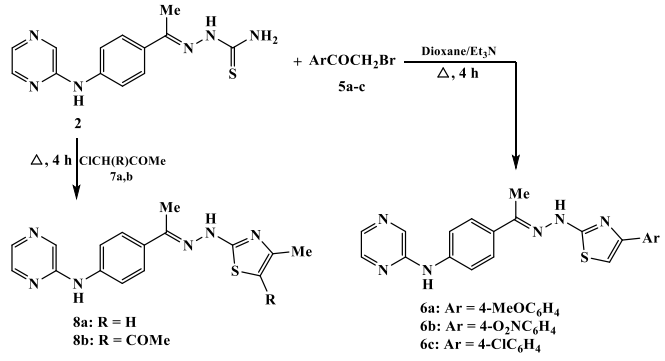

Scheme 3. Synthesis of pyrazine-thiazole analogs 6a-c and 8a-b.

boiling dioxane and triethylamine, **respectively**. The structures of pyrazine-thiazoles **6a-c** and **8a-b** were **suggested** based on their compatible data of IR, ^{1}H NMR, ^{13}C NMR, and MS analyses. The IR spectrum of pyrazine-thiazole analog **6b showed** the absorptions of the N-H groups at 3334 and 3221 cm^{-1}, while the imine group (C=N) was detected at the frequency of 1629 cm^{-1}. The ^{1}H NMR scale clearly showed the four-protons of methyl group and thiazole-C5 as singlet signals at δ 2.67 and 7.19 ppm. The aromatic protons of phenylene groups were recoded as doublet signals at δ 7.35, 7.67, 7.96, and 8.30 ppm. The pyrazine-ring`s protons of were resonated at δ 8.48 (doublet), 8.55 (doublet), and 8.64 ppm (singlet). The two-protons of N-H groups were identified at δ 9.13 and 11.83 ppm.

The proposed Hantzsch-type reaction pathway (Scheme 4) for generating pyrazine-thiazole hybrid compounds 6a-c, begins with the alkylation of the nucleophilic sulfur atom, resulting in the formation of intermediate (C). The subsequent cyclization step is driven by the nucleophilic addition of the amino group to the carbonyl group in intermediate (C), producing intermediate (D). The final products, compounds 6a-c, are obtained through the elimination of water from intermediate (D).

To pick up the fourth series of pyrazine-thiazole analogs 9 and 11a-c, the pyrazine-thiosemicarbazone 2 was subjected to the reactions with ethyl 4-chloroacetoacetate and *N*-aryl-2-oxo-propanehydrazonoyl chlorides 10a-c, respectively. The reaction of thiosemicarbazone compound 2 with ethyl 4-chloroacetoacetate was performed in boiling dioxane and triethylamine to furnish the agreeing pyrazine-thiazole conjugate 9 having ethyl acetate moiety at the position-4 of the thiazole ring (Scheme 5). Finally, treatment of thiosemicarbazone **2** with three different *N*-aryl-2-oxo-propanehydrazonoyl chlorides **10a-c** proceeded in boiling THF and triethylamine to produce the corresponding pyrazine-thiazole analogs **11a-c** substituted with arylazo group at position-5 of the thiazole skeleton. Spectral analyses were used to define the structure of the newly created pyrazine-thiazole analogs **9** and **11a-c**. The IR spectrum of **11c** indicated the absorption frequencies of N-H groups at 3328 and 3217 cm^{-1}, while the stretched band of the imine group (C=N) was detected at 1634 cm^{-1}. The ^{1}H NMR spectrum displayed two-singlet signals (δ 2.43 and 2.65 ppm), each integrated for three-protons, for the two methyl substituents. The phenylene protons were observed as doublet peaks at δ 7.26, 7.38, 7.67, and 7.75 ppm. The pyrazine ring's protons were identified as a doublet-peak at δ 8.38 ppm, another doublet-peak at δ 8.46 ppm, and a singlet-peak at δ 8.60 ppm. The two-protons of the two N-H groups exhibited more de-shielded peaks at δ 9.08 and 11.16 ppm.

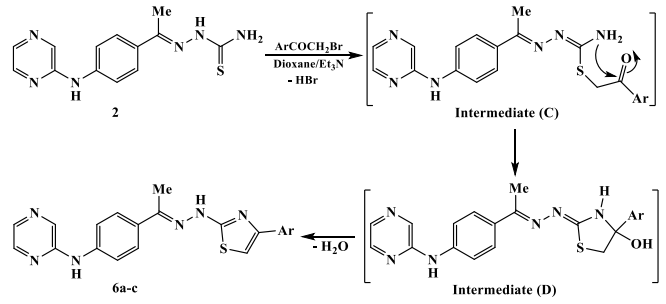

Scheme 4. Mechanism of Hantzsch-type reaction between thiosemicarbazone 2 and phenacyl bromides.

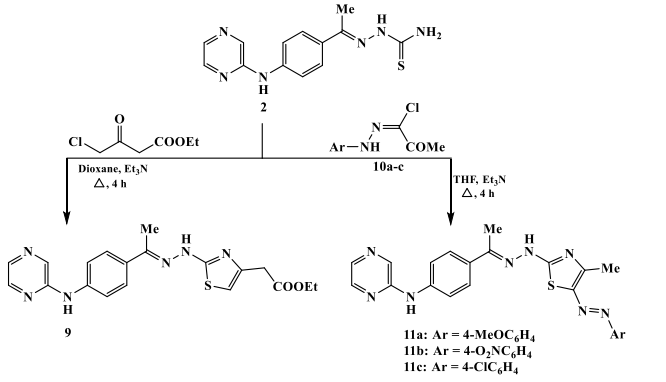

Scheme 5. Synthesis of pyrazine-thiazole analogs 9 and 11a-c.

The protons of azo-linked phenylene group in compounds 11a-c were correlated with the electronic nature of the substituent on the phenylene group. The two protons that occupy the ortho positions of the electron-donating methoxy group (compound 11a) resonated at a higher chemical shift (δ 7.01 ppm) when compared to the similar protons in compound 11b that were affected by the electron-withdrawing nitro group and resonated more de-shielded to higher chemical shift of δ 8.24 ppm.

The yields across the different pyrazine-thiazole series 4a-c, 6a-c, and 11a-c were compared to indicate the following conclusion, the pyrazine-thiazole series 4a (66.4%), 4b (71.8%), and 4c (68.1%) were obtained in showed higher yields compared to the pyrazine-thiazole series 6a (64.9%), 6b (68.4%), and 6c (61.9%) likely due to the lack of side reactions during the Knoevenagel condensation. The pyrazine-thiazole series 11a-c had relatively lower yields for 11a (55.6%), 11b (62.3%), and 11c (57.3%) attributed to steric hindrance from bulky arylazo substituent at position-5 of the thiazole ring.

3.2. Molecular modeling

The chlorobenzylidene **4c**, chlorophenyl **6c,** and azo-chlorophenyl **11c** hybrids, as representative examples of the synthesized derivatives, were submitted to DFT quantum calculations, where the suggested optimized structures have twisted configurations (Figure 2). For instance, their dihedral angles indicated that the phenylpyrazin-2-amine moiety was planar, whereas the hydrazonyl group was shifted from the phenyl's plane, e.g., $C^2_{(Ph)}$-$C^1_{(Ph)}$-$C_{(Hz)}$-$N_{(Hz)}$ = 8.5-10.2° and $C^2_{(Ph)}$-$C^1_{(Ph)}$-$C_{(Hz)}$-$Me_{(Hz)}$ = 10.8-12.4°. Also, the hydrazonyl carbon and nitrogen were strongly deviated from planarity with the thiazole ring, as $C_{(Hz)}$-$N_{(Hz)}$-$NH_{(Hz)}$-$C^2_{(Thz)}$ = 70.3-74.7° and $N_{(Hz)}$-$NH_{(Hz)}$-$C^2_{(Thz)}$-$N^3_{(Thz)}$ = 20.1-23.5°, respectively (Table S1-S3). Otherwise, the DFT bond lengths and angles in comparison to single crystal X-ray of analogs [46,47] revealed a valuable agreement as the discrepancies were <0.12 Å and <11.2° (RMSD = 0.03-0.04 and 3.9-4.6), respectively. The disparity could be ascribed to that the DFT computations investigated a sole gaseous molecule with no columbic interactions [48] (Table S2-3).

As they significantly impact the molecule's attitude to afford or receive electrons [49-52], the energies of highest occupied molecular orbital (HOMO) and lowest unoccupied molecular oribital (LUMO), FMOs, have gained noteworthy prominence. The 3D depiction of the hybrids FMOs divulged that the HOMO of **6c** and **11c** was spread over the complete molecule (π-orbital), while that of **4c** had mainly confined on the hydrazonyl aminophenyl pyrazine nucleus. Likewise, the LUMO configurations revealed that **4c** has been made up of the π*-orbital of hydrazonyl chlorobenzylidene thiazolone, while **6c** presents an alternative configuration, built from the hydrazonyl aminophenyl pyrazine π*-orbital. The derivative **11c** exhibited LUMO composed of the π*-orbital of the azochlorophenylthiazole hydrazonyl part (Figure 3). Therefore, the studied hybrids HOMO's energy (E_H) displayed related evaluates, -5.98 (**4c**), -5.60 (**6c**), and -5.57 (**11c**) eV, while the LUMO (E_L) values have been more diverse as the smallest value was observed for **6c** (-1.81 eV), whereas **4c** and **11c** exhibited the close and higher energies, -2.42 and -2.54 eV, respectively. Correspondingly, the HOMO-LUMO gap ($\Delta E_{H\text{-}L}$) fluctuated from 3.03 to 3.79 eV following the order **11c** < **4c** < **6c** (azo < chlorobenzylidene < chlorophenyl) (Table 1). Additionally, the chemical reactivity factors were assessed using the FMO's energies, namely, electronegativity (χ), global hardness (η), softness (δ), electrophilicity (ω), electron donating, and accepting powers (ω^- and ω^+) (Eqs. 1 and 2) [50].

$$\chi = -\frac{1}{2}\left(E_{HOMO} + E_{LUMO}\right) \quad \eta = -\frac{1}{2}\left(E_{HOMO} - E_{LUMO}\right) \quad \delta = \frac{1}{\eta} \tag{1}$$

$$\omega = \frac{\chi^2}{8\eta} \quad \omega^- = \frac{\left(3I + A\right)^2}{16\left(I - A\right)} \quad \omega^+ = \frac{\left(I + 3A\right)^2}{16\left(I - A\right)} \tag{2}$$

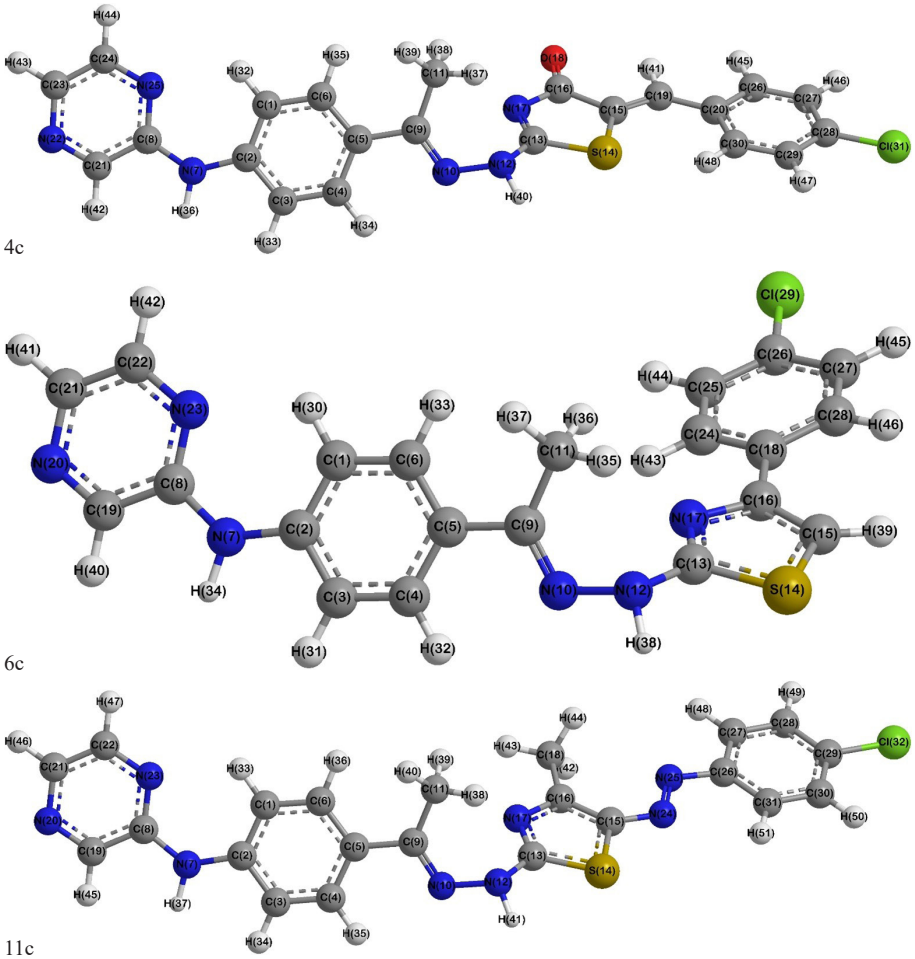

Figure 2. DFT-optimized structures of compounds 4c, 6c, and 11c, showing their electronic properties and configurations. DFT: Density functional theory.

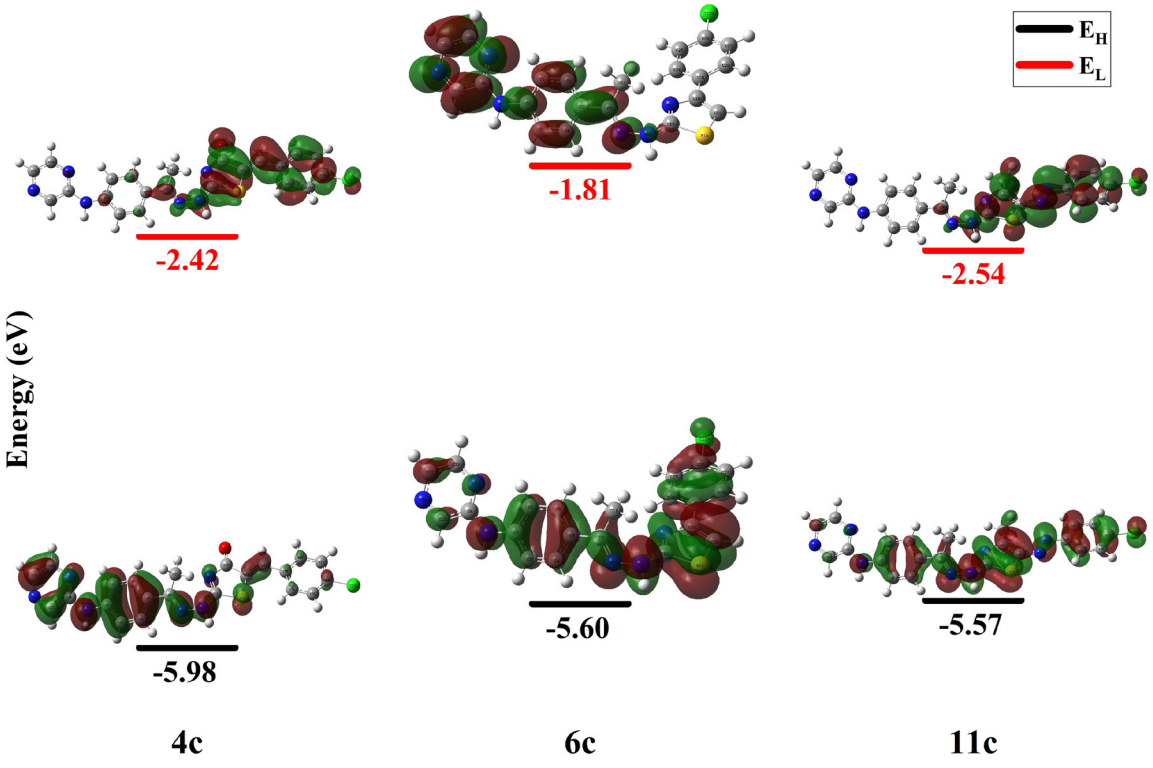

Figure 3. The 3D-plot of FMO's for compounds 4c, 6c, and 11c. FMO: Frontier molecular orbitals.

Table 1. FMO's energies and reactivity descriptors (eV) of investigated compounds.

Compound	E_H	E_L	ΔE_{H-L}	χ	η	δ	ω	ω+	ω-
4c	-5.98	-2.42	3.56	4.20	1.78	0.56	4.95	3.07	7.27
6c	-5.60	-1.81	3.79	3.70	1.89	0.53	3.62	2.00	5.70
11c	-5.57	-2.54	3.03	4.05	1.51	0.66	5.42	3.58	7.63

FMOs: Frontier molecular orbitals

The derivative **4c** exhibited the utmost electronegativity (χ) (4.20 eV), and **11c** was the softest (δ), 0.66 eV. However, **6c** presented the utmost hardness (η) (1.89 eV). The electrophilicity index (ω) has been prolonged over the 3.62-5.42 eV range. Hence, all conjugates displayed respectable electrophilicity, ω > 1.5 eV [53,54], following the **6c** < **4c** < **11c** arrangement. The electron-donating (ω^+) and acceptance (ω^-) merits unveiled more affinity to deliver than gaining electrons [53,54] (Table 1).

The examined derivatives' intramolecular charge-transfer and electronegativity have been empathized by considering Mulliken's atomic charges [55]. In all derivatives, the pyrazinyl nitrogen atoms $N^1_{(Prz)}$ and $N^4_{(Prz)}$ have gained almost matched negative charges, -0.253 - -0.254 and -0.152 – -0.153. Likewise, the phenylamine nitrogen atom -NH displayed a higher negative charge (-0.546), whereas the hydrazonyl nitrogen's $N_{(Hz)}$ and $NH_{(Hz)}$ exhibited lesser amounts, -0.221 - -0.229, and -0.416 - -0.435, respectively (Table 2). Otherwise, the thiazolyl sulfur $S^1_{(Thz)}$ and nitrogen $N^3_{(Thz)}$ had been positively and negatively charged, respectively, where **4c** presented the lowest values (0.085 and -0.229) and **6c** had the highest (0.167 and -0.269). Further, the thiazolyl carbon $C^4_{(Thz)}$ possessed a higher positive charge in **4c** (0.296) than in other derivatives (0.292 and 0.241), which could be ascribed to the electron-withdrawing effect of the attached oxo-group. Contrarily, the thiazolyl carbon $C^5_{(Thz)}$ had a negative charge and the lowest merit was observed in the azophenyl derivative **11c** (-0.158).

The sites liable for nucleophilic and electrophilic attacks have been anticipated from Fukui's indices (f_k^+ and f_k^-) [56-59]. However, Fukui's indices occasionally presented inappropriate estimates of the dynamic places. Thus, the local relative electrophilicity (s_k^- / s_k^+) and nucleophilicity (s_k^+ / s_k^-) parameters were resolved and matched with the corresponding Fukui's indices [60-62]. The electrophilic attack indices (f_k^-) of **4c**, **6c,** and **11c** presented the thiazolyl sulfur $S^1_{(Thz)}$ as the utmost active atom followed by either the chloro (Cl) or aminophenyl nitrogen (NH). In contrast, the relative electrophilicity descriptors (s_k^- / s_k^+) implied, totally altered arrangements from those gained from Fukui's indices. For instance, the aminophenyl nitrogen caught the principal site in **4c**, while the thiazolyl carbon $C^4_{(Thz)}$ and hydrazonyl nitrogen $N_{(Hz)}$ were the highest energetic sites in **6c** and **11c**, respectively (Table S4). Else, the Fukui's indices (f_k^+) suggested completely different patterns, in which the chloro (Cl), pyrazinyl nitrogen ($N^4_{(Prz)}$), and azo nitrogen ($N^1_{(Azo)}$) seized the top site in **4c**, **6c,** and **11c** conjugates, respectively. The relative nucleophilicity descriptors (s_k^+ / s_k^-) donated differed fashions of the significantly liable locations. For example, the thiazolyl ($C^4_{(Thz)}$), pyrazinyl ($C^2_{(Prz)}$), and phenyl ($C^1_{(Ph)}$) carbon atoms occupied the topmost location in hybrids **4c**, **6c,** and **11c**, respectively (Table S4).

Table 2. Selected Mulliken's atomic charges of the investigated hybrids.

Atom	4c	6c	11c	Atom	4c	6c	11c
$N^1_{(Prz)}$	-0.253	-0.254	-0.254	$S^1_{(Thz)}$	0.085	0.167	0.159
$C^2_{(Prz)}$	0.407	0.406	0.406	$C^2_{(Thz)}$	0.145	0.104	0.150
$C^3_{(Prz)}$	-0.291	-0.292	-0.292	$N^3_{(Thz)}$	-0.229	-0.269	-0.259
$N^4_{(Prz)}$	-0.152	-0.153	-0.152	$C^4_{(Thz)}$	0.296	0.292	0.241
$C^5_{(Prz)}$	-0.187	-0.189	-0.188	$C^5_{(Thz)}$	-0.184	-0.555	-0.158
$C^6_{(Prz)}$	-0.155	-0.155	-0.155	$Ox_{(Thz)}$	-0.339		
NH	-0.546	-0.546	-0.546	$CH_{(Bnz)}$	-0.250		
$C^1_{(Ph)}$	0.229	0.229	0.230	$C^1_{(Bnz)}$	0.367		
$C^4_{(Ph)}$	0.442	0.439	0.440	$C^4_{(Bnz)}$	-0.034		
$C_{(Hz)}$	0.197	0.186	0.197	$C^1_{(PhThz)}$		0.223	
$N_{(Hz)}$	-0.221	-0.229	-0.228	$C^4_{(PhThz)}$		-0.031	
$NH_{(Hz)}$	-0.416	-0.435	-0.428	$N^1_{(Azo)}$			-0.123
$Me_{(Hz)}$	-0.751	-0.754	-0.752	$N^2_{(Azo)}$			-0.204
Cl	-0.074	-0.090	-0.085	$C^1_{(PhAzo)}$			0.279
				$C^4_{(PhAzo)}$			-0.040

Additionally, the molecular polarizability (α_{total}), hyperpolarizabilities (β_{total}), and dipole moment (μ) of the inspected hybrids have been figured [63-65] to discover more about the molecule's electronic density, distribution, and softness, which fundamentally influence the intermolecular interactions (Eq. 3) [66].

$$\mu = \left(\mu_x^2 + \mu_y^2 + \mu_z^2\right)\alpha_{total} = \frac{\left(\alpha_{xx} + \alpha_{yy} + \alpha_{zz}\right)}{3}$$
$$\beta_{total} = \sqrt{\left(\beta_{xxx} + \beta_{xyy} + \beta_{xzz}\right)^2 + \left(\beta_{yyy} + \beta_{yzz} + \beta_{yxx}\right)^2 + \left(\beta_{zzz} + \beta_{zxx} + \beta_{zyy}\right)^2} \quad (3)$$

The studied hybrids exhibited a dipole moment (μ) range from 2.88 to 4.70 D, for **6c** and **11c**, which was 2.10-3.43 times more than urea's dipole [67] (Table 3). Moreover, the derivatives **6c** and **11c** presented the minimum and maximum polarizability (α_{total} = 2.65 and 3.01×10^{-23} esu), respectively. However, the first-order hyperpolarizability designated that analog **4c** disclosed the smallest merit, $\beta_{total} = 0.75\times10^{-30}$ esu, while the hybrid **11c** revealed the utmost, $\beta_{total} = 2.21\times10^{-30}$ esu. Referring to the value of urea [67], the investigated analogs presented greater hyperpolarizability (2.01-5.91 times) (Table 3).

3.3. Cytotoxic assay

The cytotoxic effectiveness on cancer and normal cells showed diverse activities of the isolated pyrazine-thiazole analogs (Figure 4 and Table S5). Analog 2 demonstrated moderate cytotoxicity toward various cancer cell lines, IC_{50} (μM): 33.02±0.42 for Panc-1, 27.67±0.21 for HepG2, and 24.03±0.18 for MCF-7, suggesting lower potency than the standard drug erlotinib. Conjugate 3 showed enhanced potency against Panc-1 cells and MCF-7 (IC_{50} = 15.49±0.09 and 20.69±0.19 μM), with very poor effectiveness towards HepG2 (IC_{50} = 30.48±0.30 μM). Meanwhile, the 4-series analogs showed significantly increased cytotoxicity. For instance, compound 4a displayed moderate inhibition against cancer cell lines, where the most significant impact was observed in MCF-7 (IC_{50} = 15.60 ± 0.07 μM). Analog 4b presented further enhancement, as its IC_{50} (μM) were ranged from 11.57 ± 0.02 (MCF-7) to 15.23 ± 0.42 (HepG2). Remarkably, the derivative 4c demonstrated outstanding effectiveness towards all tumor cell lines, showing an IC_{50} of 9.41 ± 0.33 μM for Panc-1, 10.92 ± 0.36 μM for HepG2, and 8.27 ± 0.40 μM for MCF-7. Moreover, its low activity toward WI-38 cells (IC_{50} = 83.72 ± 0.24 μM) demonstrates high selectivity and a positive therapeutic index. The 6-series hybrids also showed alternative cytotoxic effects, where their activity increased in the order of 6a < 6b < 6c, which had outstanding IC_{50} against Panc-1 (12.73 ± 0.18), HepG2 (12.80 ± 0.01), and MCF-7 (5.51 ± 0.09 μM). The conjugate 8a showed average cytotoxic effects against Panc-1 (IC_{50}=14.68±0.26) and MCF-7 (IC_{50}=18.06±0.27 μM), and lower effectiveness against HepG2 (IC_{50} = 26.49 ±0.02 μM), along with minimal impairment for WI-38 cell (IC_{50} = 88.16±0.56 μM). However, analog 8b demonstrated comparable outcomes with marginally improved specificity (Figure 4 and Table S5). In addition, compound 9 displayed significant inhibition towards Panc-1 (IC_{50} = 8.01 ± 0.23), MCF-7 (IC_{50}=17.36 ± 0.28), and HepG2 (IC_{50}=22.67 ± 0.82 μM), with moderate specificity for healthy cells. In the 11-series, 11a demonstrated moderate effectiveness against various cancer cell lines, while 11b exhibited increased effectiveness. Conversely, the hybrid 11c presented the most powerful effectiveness in this group, especially towards HepG2 (IC_{50} = 8.01 ± 0.35 μM) and MCF-7 (IC_{50}=6.62 ± 0.13 μM), indicating potential as a potent cancer-

Table 3. The dipole moment (μ; Debye), polarizability (α_{total}), polarizability anisotropy (Δα), and first-order hyperpolarizability (β_{total}) of explored hybrids (esu).

Compound	μ (Debye)	μ/μ_{urea}	α_{total} (esu×10^{-23})	Δα (esu×10^{-24})	β_{total} (esu×10^{-30})	$\beta_{total}/\beta_{urea}$
4c	4.51	3.28	2.82	2.37	0.75	2.01
6c	2.88	2.10	2.65	3.42	1.73	4.62
11c	4.70	3.43	3.01	5.31	2.21	5.91

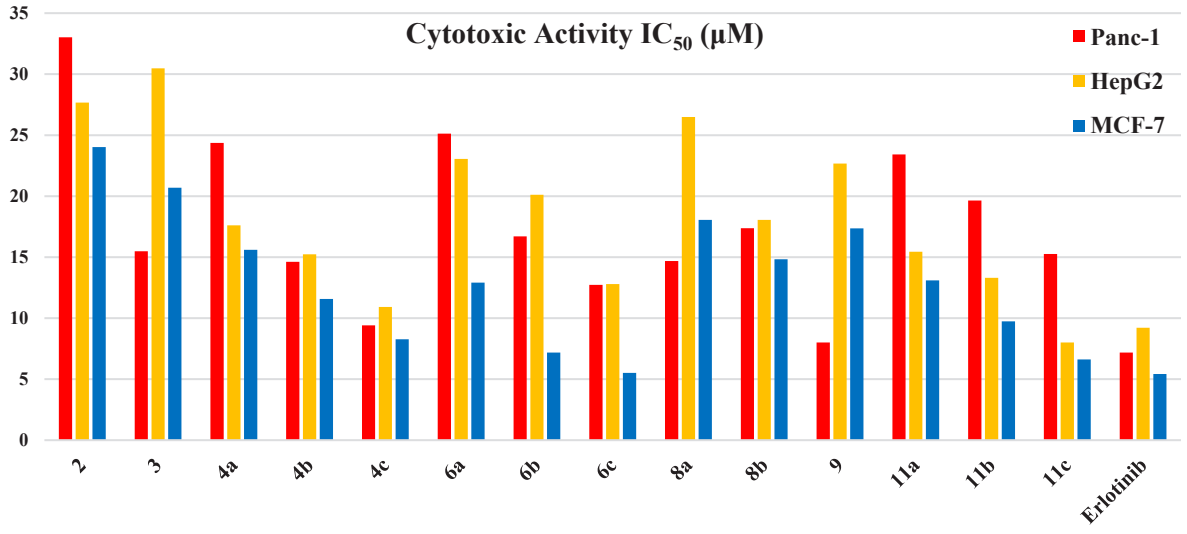

Figure 4. Cytotoxic activity of the synthesized analogs against the cancer cell lines.

fighting agent with better selectivity than erlotinib, which displayed IC_{50} = 7.18± 0.06, 9.22±0.13, 5.43±0.25 µM, against Panc-1, HepG2, and MCF-7, respectively.

3.4. Structure-activity relationship (SAR)

The SAR presented significant insights into how chemical modifications can distinctly influence the cytotoxic effectiveness of the synthesized hybrids. Based on the chemical structures, The presence of electron-withdrawing groups, such as nitro (–NO_2) and chloro (–Cl), in the chemical structures significantly boosts cytotoxic activity. This enhancement is likely attributed to increased lipophilicity and improved interactions with cellular targets. Compounds featuring methoxy (–OCH_3) groups indicate a balance between hydrophilicity and lipophilicity, influencing cellular uptake and binding interactions. Besides, the hydrazone moiety found in all synthesized compounds plays a crucial role in facilitating hydrogen bonding and electronic interactions with biological targets, thereby enhancing their activity. Among these analogs, analog 2, which contains a carbothioamide group that is intricately attached to the pyrazine-thiazole framework, exhibited a level of moderate cytotoxicity across evaluated cancer cell lines, which recommends that the existence of the carbothioamide group offers a modest contribution to the overall cytotoxic activity. In contrast, derivative 3, which incorporates a thiazol-4-one moiety as part of its chemical structure, displayed a notable improvement in cytotoxicity, particularly against the Panc-1 cell line, thereby indicating that the thiazol-4-one group significantly enhances the anti-cancer efficacy when compared to the earlier mentioned carbothioamide. However, within the 4-series, the presence of various benzylidene substitutions had a considerable impact on the potency of the analogs, demonstrating that even slight variations in chemical structure can lead to substantial differences in the cytotoxic effectiveness. For instance, compound 4a, which possessed a methoxy-benzylidene substitution, exhibited a moderate level of efficacy in its cytotoxic effects, thereby highlighting how particular modifications can influence the effectiveness of these analogs in targeting cancer cells. Characterized by the presence of a nitro-benzylidene substitution, 4b exhibited a significantly enhanced level of potency across a diversity of tumor cell lines, thereby suggesting that the incorporation of the electron-withdrawing moiety such as nitro group may indeed have a positive effect on the overall cytotoxicity of the analog. In contrast, the 4c, with chloro-benzylidene group, demonstrated the highest level of efficacy within this series of analogs, thereby highlighting the notion that the presence of the chloro group likely bestows superior cytotoxic effectiveness, which can be attributed to its increased lipophilicity coupled with its electron-donating properties that enhance the compound's interaction with cellular targets. Meanwhile, the 6-series analogs feature a thiazole ring modified with diverse substituents, thus creating a diverse array of analogs for evaluation. For example, hybrid 6a, having a methoxyphenyl group, exhibited a moderate level of potency, particularly notable against the MCF-7 cell line, reflecting its potential therapeutic relevance. However, analog 6b, incorporating a nitrophenyl substitution, presented a stronger level of efficacy against MCF-7, further reinforcing the hypothesis that electron-withdrawing groups play a critical role in enhancing cytotoxic effects. Lastly, 6c, characterized by its chlorophenyl substitution, achieved the highest potency within this specific series of analogs, which once again emphasizes the beneficial influence of the chloro-group on the overall cytotoxic performance. The 8-series incorporate methyl-thiazole substitutions, where the derivative 8a exhibited moderate activity across cancer cell lines, while the 8b, featured by an acetyl-thiazole group, demonstrated comparable potency, suggesting that acetyl-thiazole substitutions confer moderate, balanced cytotoxicity. Moreover, analog 9, ethyl-thiazole-acetate ester, showed strong potency against Panc-1, indicating that the ester group improves cytotoxicity, possibly by enhancing cellular uptake. Furthermore, the 11-series conjugates contained diazinyl linked to variously substituted thiazole, wherein the hybrid 11a, with a methoxyphenyl-diazenyl group, demonstrated moderate efficacy for MCF-7. Further, 11b with a nitrophenyl-diazenyl group, showed increased potency for MCF-7, suggesting that the nitro group enhances activity, whereas 11c, incorporating a chlorophenyl-diazenyl group, exhibited the strongest cytotoxicity in this series, particularly against MCF-7, confirming that chlorinated substitutions are highly beneficial for improving anti-cancer efficacy. Overall, the SAR analysis highlights that electron-withdrawing groups like nitro and chloro, particularly on the benzylidene and diazenyl-linked thiazole rings, significantly enhance cytotoxicity. The thiazole ring substitutions and ester functionality also contribute to improved activity, while methoxy groups confer moderate efficacy. These results suggest structural modifications that can be optimized to enhance the anti-cancer potential of pyrazine-thiazole analogs.

3.4.1. The therapeutic index (TI)

The therapeutic index (TI) is a key parameter for assessing the safety and efficiency of a drug. It is classically defined as the ratio of the IC_{50} for normal cells to the IC_{50} for cancer cells. A higher TI indicates a greater selectivity and safety profile of the compound.

3.4.2. Estimation of therapeutic index

Based on the cytotoxicity data provided in this work, through the Normal Cell Line (WI-38), the IC_{50} values of analogs like 6c and 11c against WI-38 were relatively high (e.g., analog 6c has IC50 = 83.72 ± 0.24 µM),

indicating low toxicity to normal cells. Meanwhile, across the Cancer Cell Lines For MCF-7, analog 6c exhibited an IC_{50} of 5.51 ± 0.09 μM, and analog 11c exhibited an IC_{50} of 6.62 ± 0.13 μM. However, analog 6c and 11c had IC_{50}s of 12.80 ± 0.01 μM, and IC_{50} of 8.01 ± 0.35 μM for HepG2.

3.4.3. Therapeutic index calculation

The TI were calculated for the promising analogs, such as 6c and 11c. TI for 6c: MCF-7 = 83.72/ 5.51=15.2; HepG2 = 83.72/12.80=6.54. TI for analog 11c: MCF-7 = 83.72/6.62=12.64; HepG2 = 83.72/8.01=10.45.

Insight into the TIs for analog 6c and 11c is promising and indicates selective cytotoxicity against cancer cells with limited effects on normal cells. Analog 6c shows the highest TI for MCF-7 (15.2), demonstrating its significant selectivity for breast cancer cells compared to normal cells. Analog 11c has slightly lower TI values than analog 6c but still demonstrates favorable selectivity, particularly for HepG2 (TI = 10.45). The high TI of analog 6c may be attributed to its chlorophenyl substitution, which enhances cytotoxicity in cancer cells while sparing normal cells. Chlorophenyl groups can improve lipophilicity, enhancing interactions with cancer-specific targets. Similarly, analog 11c, with its chlorophenyl-diazenyl substitution, shows excellent selectivity, likely due to its ability to selectively inhibit CA isoforms in tumor cells, which are less expressed in normal cells. Furthermore, the IC_{50} of erlotinib against cancer cells is similar to these analogs. However, its toxicity to normal cells (not specified in the manuscript) might be higher, suggesting that these compounds could offer a better therapeutic index than erlotinib. Finally, analogs 6c and 11c exhibit high TIs, especially against MCF-7 and HepG2 cells, suggesting their potential as safe and selective anti-cancer agents. Future *in vivo* studies are recommended to validate these findings and to explore their pharmacokinetic and pharmacodynamic profiles.

3.5. Carbonic anhydrase assay

The differences in potency and selectivity were emphasized by the inhibition results of the pyrazine-thiazole analogs against *CA IX* and *CAXII* due to structural variations (Table 4). Analogu **2** demonstrated moderate inhibition towards both *CAIX* (IC_{50}= 0.22 ± 0.0333) and *CAXII* (IC_{50} = 0.208 ± 0.007 μM)**,** exhibiting similar effectiveness but less strength over AZA. Alternatively, derivative 3, which includes a thiazol-4-one moiety as part of its chemical structure, showed remarkable specificity for *CAIX* (IC_{50} = 0.014 ± 0.045 μM), which is the strongest inhibition seen among all analogs toward *CAIX*. Nevertheless, its effect against *CAXII* enzyme was found to be moderate (IC_{50} = 0.372 ± 0.065 μM), suggesting that this analog could be a specific blocker for the *CAIX* enzyme. However, the 4-series conjugates demonstrated significant activity on both isoforms. Although the hybrid 4a (IC_{50}=0.078 ± 0.053) had a balanced inhibition profile, 4b displayed enhanced inhibition even more (IC_{50}=0.089 ± 0.061 μM) comparable with the AZA. However, derivative **4c** stood out as a highly effective inhibitor within the series, IC_{50} = 0.052 ± 0.014 (for *CAIX*) and 0.091 ± 0.018 μM (for *CA XII*). The **6**-series analogs showed moderate inhibition profiles, where 6a exhibited IC_{50} values 0.096 ± 0.038 and 0.568 ± 0.042 μM towards *CAIX* and *CAXII*, respectively, indicating its superior effectiveness for *CAIX*. Similarly, hybrids 6b-c displayed very weak effectiveness against *CAXII* and moderate against *CAIX*, indicating limited inhibition for both isoforms. Within the 8-series, compound 8a exhibited equal suppression, while 8b demonstrated comparable effectiveness (IC_{50} =0.081 ± 0.062 and 0.090 ± 0.033 μM for *CA IX* and *CA XII*, correspondingly). Moreover, compound 9 presented moderate effectiveness, indicating decent inhibition but slightly weaker strength compared to other analogs. The derivative 11a, in 11-series, had **a**n IC_{50} = 0.075 ± 0.006 μM for *CAIX* and 0.159 ± 0.002 μM for *CAXII*, whereas analog **11b** displayed strong inhibition, especially against *CAIX* over an IC_{50} = 0.068 ± 0.023 μM. The hybrid **11c** disclosed moderate effectiveness (IC_{50} = 0.098 ± 0.036 μM for *CAIX* and 0.101 ± 0.029 μM for *CAXII*), indicating a good balance. Finally, conjugates **4c, 4b,** and **11b** showed comparable *CAIX* and *CAXII* inhibition compared to AZA **(IC_{50} = 0.062** ± 0.014 and 0.080 ± **0.013 μM).**

Table 4. Carbonic anhydrase inhibitions of the prepared analogs (IC_{50} in μM).

Analogs	*CAIX*	*CAXII*
2	0.223 ±0.033	0.208 ±0.007
3	0.014 ±0.045	0.372 ±0.065
4a	0.106 ±0.030	0.086 ±0.007
4b	0.078 ±0.053	0.089 ±0.061
4c	0.052 ±0.014	0.091 ±0.018
6a	0.096 ±0.038	0.568 ±0.042
6b	0.154 ±0.029	0.764 ±0.023
6c	0.131 ±0.049	0.989 ±0.011
8a	0.097 ±0.028	0.134 ±0.007
8b	0.081 ±0.062	0.09 ±0.033
9	0.162 ±0.011	0.204 ±0.045
11a	0.075 ±0.006	0.159 ±0.002
11b	0.068 ±0.023	0.132 ±0.004
11c	0.098 ±0.036	0.101 ±0.029
AZA	0.062 ±0.014	0.080 ±0.013

AZA: Acetazolamide

3.5.1. Acetazolamide (AZA) as carbonic anhydrase reference

The biological efficacy of the synthesized pyrazine-thiazole analogs is closely associated with their structural characteristics, which play a crucial role in determining both cytotoxicity and inhibition of carbonic anhydrase. The presence of electron-withdrawing groups, such as nitro (NO_2) and chloro (Cl), significantly boosts cytotoxic activity by enhancing the lipophilicity of the compounds, thereby promoting stronger interactions with cancer-specific targets. For example, compound 6c, featuring a chlorophenyl substitution, demonstrated the highest potency against MCF-7 cells (IC_{50} = 5.51 ± 0.09 μM) due to its improved hydrophobic interactions and electronic properties. In contrast, electron-donating groups like methoxy (OCH_3), present in compounds 4a and 6a, provide moderate activity by achieving a balance between hydrophilicity and lipophilicity, which influences cellular uptake and binding efficiency. Additionally, the thiazole ring acts as a rigid scaffold that improves spatial orientation and allows for functional group diversification. These structural attributes also affect CA isoform selectivity, with compounds like 3 exhibiting strong inhibition of CAIX (IC_{50} = 0.014 ± 0.045 μM) due to the interaction of the thiazolin-4-one moiety with the enzyme's active site. Substitutions, such as chlorobenzylidene and chlorophenyl in compounds like 4c and 11c, respectively, strengthen interactions with the hydrophobic regions of CA isoforms, resulting in effective dual inhibition of CAIX and CAXII. Collectively, these insights highlight that the strategic combination of specific functional groups and structural designs enhances the biological activity of these analogs, positioning them as promising candidates for selective and potent anti-cancer therapies.

3.6. Molecular docking

The molecular docking showed a variety of interaction affinities and patterns for the pyrazine-thiazole derivatives with the 6CB0 receptor (Table S6). Derivative **2** had the lowest affinity (-6.1099 kcal/mol), interacting through hydrogen donor and acceptor bonds with Glu123 and Lys152**,** in addition to a π-H interaction with Trp52 (Figure S1). However, **compound 3** had a slightly higher affinity (-7.0020 kcal/mol), forming a hydrogen bond with Arg205 (Figure S1). Meanwhile, the 4-series derivatives had higher affinities, where 4b presented affinity of -8.1523 kcal/mol, *via* multiple hydrogen donor bonds with Arg205 and Glu44, while 4a exhibited stabilizing π-cation interactions (Figure 5). Derivative **4c** showed a moderate affinity (-7.9394 kcal/mol), which may be attributed to the phenyl substitution affecting its interaction profile. All derivatives of the 6-series interacted with Arg205 (Figure S1), and 6b had the highest affinity (-8.2382 kcal/mol) by creating a stable hydrogen donor bond with Arg205, while **6a** and **6c** displayed scores -7.8517 and -7.9533 kcal/mol, respectively (Figure 5). Moreover, in the 8-series, the conjugates 8a and 8b formed multiple hydrogen bonds with Arg 20 through their thiazole rings (Figure S1). However, derivative 9 had a unique interaction pattern, engaging with Ser179 and Lys152 through hydrogen bonds and π-cation interactions, achieving a score = -7.7557 kcal/mol. Furthermore, the derivatives of 11-series showed strong binding abilities, where 11b exhibited the

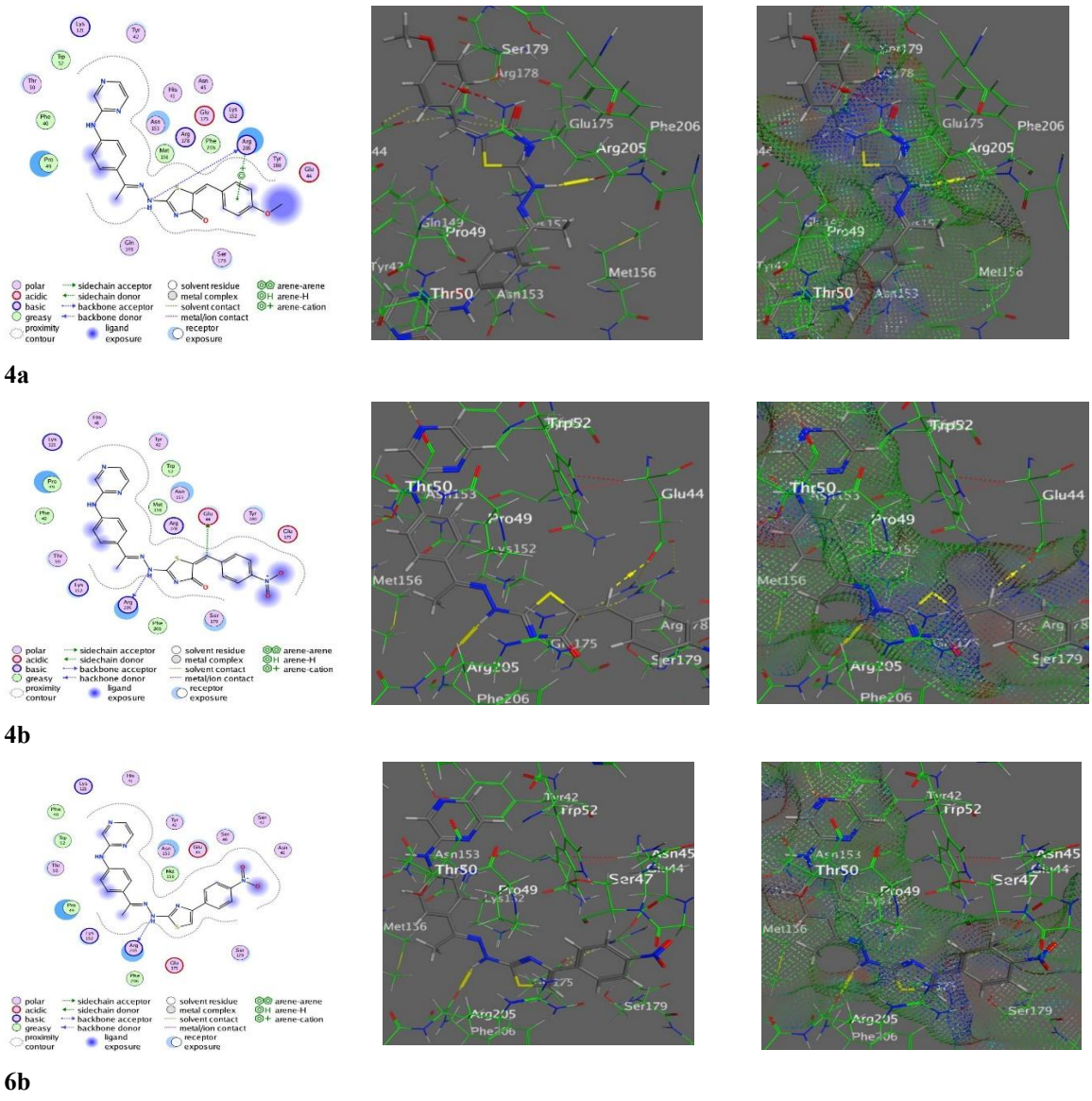

Figure 5. Docking images of 4a-b and 6b with the PDB: 6CB0 amino acid.

highest score (-8.5010 kcal/mol), by forming hydrogen donor and acceptor bonds with Arg205 and Lys121, respectively. Analogs **11a** and **11c** also had high docking scores through stabilizing hydrogen and π-cation interactions with Arg205 and other residues. Besides, the reference drug (erlotinib) presented a score of -7.0792 kcal/mol, by hydrogen bonding with Lys152, but several synthesized derivatives, such as **11b**, **4b**, and **6b**, surpassed its binding strength (Figure S1).

3.7. Pharmacokinetic properties

The SwissADME analyses demonstrated different characteristics for the analogs under study (Figure S2 and Table S7). Analog **2** had a molecular weight (M. Wt.) of 286.36 which has three hydrogen-donors (H-BD) and three hydrogen-acceptors (H-BA), with good GI absorption, good solubility, and a bioavailability score of 0.55. There was a significant increase in the MW of analog **3** (326.38), but the absorption and solubility properties were comparable, and it had a good drug-likeness score and no Lipinski violations. In the 4-series analogs, **4a-c** possessed better pharmacometrics profiles, while analog **4a** (M. Wt. = 444.51) exhibited good GI absorption and solubility. However, **4b** registered high TPSA (162.75 Å^2) among the series, which might affect permeability, but absorption and solubility were good. In addition, analog **4c** had a TPSA of 116.93 Å^2 which is beneficial, as it possibly increases the drug's bioavailability and paves the way for further development. Meanwhile, the 6-series analogs, such as **6a**, **6b,** and **6c** were of moderate solubility and had other M. Wt. values in the range of 416.5 and 431.47. Analog **6a** on the other hand, displayed superb GI absorption and relatively higher iLOGP (3.08) values indicating high lipophilicity. However, **6b** and **6c** have shown lower GI absorption, indicating that a modification in the structure may be necessary to increase their permeability and bioavailability. However, the 8-series analogs exhibited moderate solubility and were highly GI-absorbed. Analog **8a** (M. Wt. = 324.4) obtained a TPSA of 103.33 Å^2, which implies good oral bioavailability. Likewise, **8b** continued to show high level of absorption showing that the drug kinetics are consistent in this series. In the 9-series analog, a molecular weight of 396.47 and several rotatable bonds (9) were noticed, which might affect its pharmacokinetics. Despite these features, the analog had high and efficient absorption and moderate solubility with a bioavailability score equal to 0.55. The various analogs within the 11-series displayed a range of unique and distinct characteristics, with **11a** and **11c** specifically demonstrating notably poor solubility coupled with low GI absorption, which strongly implies a pressing need for further optimization and refinement to enhance their overall efficacy and performance. In contrast, analog **11b**, which possesses a molecular weight of 473.51 and boasts the highest total polar surface area of 173.87 Å^2 among all

the examined analogs, exhibited a certain level of promise despite its classification as poorly soluble, suggesting that there may be potential for its application in pharmaceutical contexts. Additionally, the bio-availability score (0.55) indicates a favorable rank of drug-likeness, which is a positive attribute for any compound intended for therapeutic use, although it is worth noting that one violation of Lipinski's rules was recorded, thereby indicating that there remains considerable opportunity for structural refinement and optimization to improve its viability as a drug candidate. Overall, the findings surrounding these analogs highlight the challenges and opportunities that lie ahead in the quest for developing effective pharmaceutical agents that can overcome existing limitations in solubility and absorption characteristics.

4. Conclusions

The synthetic strategy of targeting the pyrazine-linked thiazole analogs **3**, **4**, **6**, **8**, **9**, and **11**, was based on the interaction between the thiosemicarbazone (**2**) derived from 2-(4-acetylphenyl)amino-pyrazine (**1**) and several halo-carbonyl reagents (namely; chloroacetic acid, phenacyl bromides, chloroacetone, 4-chloroacetylacetone, ethyl 4-chloroacetoacetate, and/or *N*-aryl-2-oxo-propanehydrazonoyl chlorides). The studied hybrids displayed alternative configurations of their HOMO and LUMO. Thus, the FMO's gap ($\Delta E_{H\text{-}L}$), were in the range of 3.03-3.79 eV, resulting in the order **11c** < **4c** < **6c** (azo < chlorobenzylidene < chlorophenyl). However, the first-order hyperpolarizability designated that all studied compounds had superior hyperpolarizability than urea, by 2.01-5.91 times. Meanwhile, the evaluation of cytotoxicity for the newly synthesized analogs found a few strong contenders with effective and specific anti-cancer properties. Derivative **4c** stood out as a primary analog because of its potent killing effect on all cancer cells, especially against HepG2 (IC_{50} = 10.92 ± 0.36 µM) and low harm to healthy cells. Similarly, conjugates **6c** (IC_{50} = 5.51 ± 0.09) and **11c** (IC_{50} = 6.62±0.13 µM) showed strong effectiveness, especially against MCF-7. Thus, such hybrids, **4c, 6c,** and **11c,** displayed considerable promise as cancer-fighting agents. Furthermore, the inhibition of carbonic anhydrase presented some of the pyrazine-thiazole analogs as potential inhibitors targeting *CAIX* and *CAXII* with specific or equal inhibition characteristics. For instance, the derivative 3 was a remarkable selective inhibitor of *CAIX*, while 4c, 4b, and 11b exhibited significant inhibition of both isoforms. It concluded that strong CA isoform inhibition and selective cytotoxicity of analogs, chiefly hybrids 6c and 11c, highlight their potential for cancer therapy. Moreover, the molecular docking indicated that several synthesized conjugates have advantageous binding interactions with the 6CB0 receptor, superior to the reference drug erlotinib. Compound 11b appeared as the most promising candidate *via* establishing robust hydrogen donor and acceptor interactions with critical residues. Analogs **4b** and **6b** exhibited significant binding affinities, suggesting their potential as therapeutic agents. These results underscore the potential of pyrazine-thiazole analogs for further refinement and development in therapeutic strategies targeting the 6CB0 receptor. Eventually, the SwissADME brings to light the highly promising pharmacokinetic characteristics of the synthesized pyrazine-thiazoles, where the **4a-c** analogs have emerged as exceptionally strong contenders due to their remarkable levels of absorption and solubility, which are critical factors for drug efficacy. The 6 and 8-series showcased a well-balanced profile, thereby reinforcing their potential for effective oral drug delivery, which is an essential consideration in pharmacology.

CRediT authorship contribution statement

Khadra B. Alomari, Hind A. Siddiq: Data curation, formal analysis, methodology, and software; **Jihan Qurban, Abdulmajeed F. Alrefaei:** Investigation and writing – review & editing; **Abrar Bayazeed, Nawaa Ali H. Alshammari:** formal analysis, investigation, writing-original draft. **Hanadi A. Katouah, and Nashwa M. El-Metwaly:** Supervision and administration of research group.

Data availability

All relevant data are within the manuscript and available from the corresponding author upon request.

Declaration of competing interest

The authors declare that they have no competing interests.

Declaration of Generative AI and AI-assisted technologies in the writing process

The authors confirm that there was no use of artificial intelligence (AI)-assisted technology for assisting in the writing or editing of the manuscript and no images were manipulated using AI.

Supplementary data

Supplementary material to this article can be found online at https://dx.doi.org/10.25259/AJC_300_2024.

References

1. Francies, F.Z., Hull, R., Khanyile, R., Dlamini, Z. 2020. Breast cancer in low-middle income countries: abnormality in splicing and lack of targeted treatment options. *American Journal of Cancer Research* **10**, 1568-91.
2. Costa, B., Amorim, I., Gärtner, F., Vale, N., 2020. Understanding breast cancer: From conventional therapies to repurposed drugs. *European Journal of Pharmaceutical Sciences* **151**, 105401. https://doi.org/10.1016/j.ejps.2020.105401
3. Ganesan, K., Du, B., Chen, J., 2022. Effects and mechanisms of dietary bioactive compounds on breast cancer prevention. *Pharmacological Research* **178**, 105974. https://doi.org/10.1016/j.phrs.2021.105974
4. Malik, J., Ahmed, S., Jan, B., Bender, O., Al Hagbani, T., Alqarni, A., Anwar, S., 2022. Drugs repurposed: An advanced step towards the treatment of breast cancer and associated challenges. *Biomedicine & Pharmacotherapy* **145**, 112375. https://doi.org/10.1016/j.biopha.2021.112375
5. Manzari, M., Shamay, Y., Kiguchi, H., Rosen, N., Scaltriti, M., Heller, D., 2021. Targeted drug delivery strategies for precision medicines. *Nature Reviews Materials* **6**, 351-370. https://doi.org/10.1038/s41578-020-00269-6
6. Li, K., Du, Y., Li, L., Wei, D., 2020. Bioinformatics approaches for anti-cancer drug discovery. *Current Drug Targets* **21**, 3-17. https://doi.org/10.2174/1389450120666190923162203
7. Supuran, C., 2023. Targeting carbonic anhydrases for the management of hypoxic metastatic tumors. *Expert Opinion on Therapeutic Patents* **33**, 701-720. https://doi.org/10.1080/13543776.2023.2245971
8. Zamanova, S., Shabana, A., Mondal, U., Ilies, M., 2019. Carbonic anhydrases as disease markers. *Expert Opinion on Therapeutic Patents* **29**, 509-533. https://doi.org/10.1080/13543776.2019.1629419
9. Nocentini, A., Donald, W.A., Supuran, C.T. 2019. Human carbonic anhydrases: tissue distribution, physiological role, and druggability, Carbonic anhydrases, Elsevier, p. 151-185.
10. Di Fiore, A., Supuran, C., Scaloni, A., De Simone, G., 2022. Post-translational modifications in tumor-associated carbonic anhydrases. *Amino Acids* **54**, 543-558. https://doi.org/10.1007/s00726-021-03063-y
11. Becker, H., 2020. Carbonic anhydrase IX and acid transport in cancer. *British Journal of Cancer* **122**, 157-167. https://doi.org/10.1038/s41416-019-0642-z
12. Xiao-Qun, Z., Xian-Li, M., Ariffin, N., 2024. The potential of carbonic anhydrase enzymes as a novel target for anti-cancer treatment. *European Journal of Pharmacology* **976**, 176677. https://doi.org/10.1016/j.ejphar.2024.176677
13. Chauhan, A., Salahuddin, , Mazumder, A., Kumar, R., Ahsan, M.J., Yar, M.S., Kumar, A., Kapoor, B., 2025. Innovative synthesis of 3,5-disubstituted pyrazoline with heterocyclic system for hybrid development. *Letters in Organic Chemistry* **22**, 263-282. https://doi.org/10.2174/0115701786329318240925115206
14. Ren, A., Zhang, Y., Bian, Y., Liu, Y., Zhang, Y., Ren, C., Zhou, Y., Zhang, T., Feng, X., 2024. Pyrazines in food samples: Recent update on occurrence, formation, sampling, pretreatment and analysis methods. *Food Chemistry* **430**, 137086. https://doi.org/10.1016/j.foodchem.2023.137086
15. Chen, G.-Q., Guo, H.-Y., Quan, Z.-S., Shen, Q.-K., Li, X., Luan, T., 2023. Natural products-Pyrazine hybrids: A review of developments in medicinal chemistry. *Molecules* **28**, 7440. https://doi.org/10.3390/molecules28217440
16. Fayek, N., Xiao, J., Farag, M., 2023. A multifunctional study of naturally occurring pyrazines in biological systems; formation mechanisms, metabolism, food applications and functional properties. *Critical Reviews in Food Science and Nutrition* **63**, 5322-5338. https://doi.org/10.1080/10408398.2021.2017260
17. Garrido, A., Vera, G., Delaye, P.-O., Enguehard-Gueiffier, C., 2021. Imidazo [1, 2-b] pyridazine as privileged scaffold in medicinal chemistry: An extensive review. *European Journal of Medicinal Chemistry* **226**, 113867. https://doi.org/10.1016/j.ejmech.2021.113867
18. Choudhary, D., Garg, S., Kaur, M., Sohal, H.S., Malhi, D.S., Kaur, L., Verma, M., Sharma, A., Mutreja, V., 2023. Advances in the synthesis and bio-applications of pyrazine derivatives: A review. *Polycyclic Aromatic Compounds* **43**, 4512-4578. https://doi.org/10.1080/10406638.2022.2092873
19. Sahu, R., Shah, K., Gautam, Y., Sahu, K., 2023. Pyrazine moiety: Recent developments in cancer treatment. *Current Organic Chemistry* **27**, 821-843. https://doi.org/10.2174/1385272827666230816105317
20. Alsfouk, A., 2024. Pyrazine-based small molecule kinase inhibitors: Clinical applications and patent review (2019-2023). *Future Medicinal Chemistry* **16**, 1899-1921. https://doi.org/10.1080/17568919.2024.2385293

21. Ebenezer, O., Jordaan, M., Carena, G., Bono, T., Shapi, M., Tuszynski, J., 2022. An overview of the biological evaluation of selected nitrogen-containing heterocycle medicinal chemistry compounds. *International Journal of Molecular Sciences* **23**, 8117. https://doi.org/10.3390/ijms23158117
22. Mermer, A., Keles, T., Sirin, Y., 2021. Recent studies of nitrogen containing heterocyclic compounds as novel antiviral agents: A review. *Bioorganic Chemistry* **114**, 105076. https://doi.org/10.1016/j.bioorg.2021.105076
23. Makhova, N.N., Belen'kii, L.I., Gazieva, G.A., Dalinger, I.L., Konstantinova, L.S., Kuznetsov, V.V., Kravchenko, A.N., Krayushkin, M.M., Rakitin, O.A., Starosotnikov, A.M., Fershtat, L.L., Shevelev, S.A., Shirinian, V.Z., Yarovenko, V.N., 2020. Progress in the chemistry of nitrogen-, oxygen- and sulfur-containing heterocyclic systems. *Russian Chemical Reviews* **89**, 55-124. https://doi.org/10.1070/rcr4914
24. Sharma, P., Bansal, K., Sharma, A., Sharma, D., Deep, A., 2020. Thiazole-containing compounds as therapeutic targets for cancer therapy. *European Journal of Medicinal Chemistry* **188**, 112016. https://doi.org/10.1016/j.ejmech.2019.112016
25. Othman, I., Alamshany, Z., Tashkandi, N., Gad-Elkareem, M., Abd El-Karim, S., Nossier, E., 2021. Synthesis and biological evaluation of new derivatives of thieno-thiazole and dihydrothiazolo-thiazole scaffolds integrated with a pyrazoline nucleus as anticancer and multi-targeting kinase inhibitors. *RSC Advances* **12**, 561-577. https://doi.org/10.1039/d1ra08055e
26. Borcea, A., Ionuț, I., Crișan, O., Oniga, O., 2021. An overview of the synthesis and antimicrobial, antiprotozoal, and antitumor activity of thiazole and bisthiazole derivatives. *Molecules* **26**, 624. https://doi.org/10.3390/molecules26030624
27. Petrou, A., Fesatidou, M., Geronikaki, A., 2021. Thiazole ring\u2014A biologically active scaffold. *Molecules* **26**, 3166. https://doi.org/10.3390/molecules26113166
28. Shareef, M.A., Khan, I., Babu, B.N., Kamal, A., 2020. A comprehensive review on the therapeutic versatility of imidazo [2,1-b]thiazoles. *Current Medicinal Chemistry* **27**, 6864-6887. https://doi.org/10.2174/0929867326666190729152440
29. Singh, A., Malhotra, D., Singh, K., Chadha, R., Bedi, P.M.S., 2022. Thiazole derivatives in medicinal chemistry: Recent advancements in synthetic strategies, structure activity relationship and pharmacological outcomes. *Journal of Molecular Structure* **1266**, 133479. https://doi.org/10.1016/j.molstruc.2022.133479
30. Alizadeh, S., Hashemi, S., 2021. Development and therapeutic potential of 2-aminothiazole derivatives in anticancer drug discovery. *Medicinal Chemistry Research* **30**, 771-806. https://doi.org/10.1007/s00044-020-02686-2
31. Cascioferro, S., Parrino, B., Carbone, D., Schillaci, D., Giovannetti, E., Cirrincione, G., Diana, P., 2020. Thiazoles, their benzofused systems, and thiazolidinone derivatives: Versatile and promising tools to combat antibiotic resistance. *Journal of Medicinal Chemistry* **63**, 7923-7956. https://doi.org/10.1021/acs.jmedchem.9b01245
32. Bera, P., Aher, A., Brandao, P., Manna, S.K., Bhattacharyya, I., Mondal, G., Jana, A., Santra, A., Bera, P., 2021. Anticancer activity, DNA binding and docking study of M (ii)-complexes (M=Zn, Cu and Ni) derived from a new pyrazine–thiazole ligand: Synthesis, structure and DFT. *New Journal of Chemistry* **45**, 11999-12015. https://doi.org/10.1016/j.saa.2011.05.052
33. Bera, P., Aher, A., Brandao, P., Manna, S.K., Mondal, G., Jana, A., Santra, A., Jana, H., Bera, P., 2020. Induced apoptosis against U937 cancer cells by fe(II), co(III) and ni(II) complexes with a pyrazine-thiazole ligand: Synthesis, structure and biological evaluation. *Polyhedron* **182**, 114503. https://doi.org/10.1016/j.poly.2020.114503
34. Tan, X.-J., Liu, H.-Z., Ye, C.-Z., Lou, J.-F., Liu, Y., Xing, D.-X., Li, S.-P., Liu, S.-L., Song, L.-Z., 2014. Synthesis, characterization and in vitro cytotoxic properties of new silver(I) complexes of two novel schiff bases derived from thiazole and pyrazine. *Polyhedron* **71**, 119-132. https://doi.org/10.1016/j.poly.2014.01.014
35. Kumari, G., Dhillon, S., Rani, P., Chahal, M., Aneja, D., Kinger, M., 2024. Development in the synthesis of bioactive thiazole-based heterocyclic hybrids utilizing phenacyl bromide. *ACS Omega* **9**, 18709-18746. https://doi.org/10.1021/acsomega.3c10299
36. Frisch, M., Trucks, G., Schlegel, H., Scuseria, G., Robb, M., Cheeseman, J., Scalmani, G., Barone, V., Mennucci, B., Petersson, G., 2009. Gaussian 09W, Gaussian. Inc., Wallingford, CT, USA.
37. Becke, A.D., 1993. Density-functional thermochemistry. III. The role of exact exchange. *The Journal of Chemical Physics* **98**, 5648-5652.
38. Lee, C., Yang, W., Parr, R., 1988. Development of the colle-salvetti correlation-energy formula into a functional of the electron density. *Physical Review. B, Condensed Matter* **37**, 785-789. https://doi.org/10.1103/physrevb.37.785
39. Perdew, J., Wang, Y., 1992. Pair-distribution function and its coupling-constant average for the spin-polarized electron gas. *Physical Review. B, Condensed Matter* **46**, 12947-12954. https://doi.org/10.1103/physrevb.46.12947
40. Dennington, R., Keith, T., Millam, J., 2009, GaussView, version 5, Semichem Inc., Shawnee Mission, KS.
41. Delley, B., 2006. Ground-state enthalpies: Evaluation of electronic structure approaches with emphasis on the density functional method. *The Journal of Physical Chemistry A* **110**, 13632-13639. https://doi.org/10.1021/jp0653611
42. Biovia, D.S., 2017. Materials Studio, Dassault Systèmes, San Diego.
43. Abdel-latif, E., Abdel-fattah, S., Gaffer, H.E., Etman, H.A., 2016. Synthesis and antitumor activity of some new pyrazolo[3,4-d]pyrimidine and pyrazolo[3,4-b] pyridine derivatives. *Egyptian Journal of Basic Applied Science* **3**, 118-124. https://doi.org/10.1016/j.ejbas.2015.11.001
44. Akocak, S., Güzel-Akdemir, Ö., Kishore Kumar Sanku, R., Russom, S., Iorga, B., Supuran, C., Ilies, M., 2020. Pyridinium derivatives of 3-aminobenzenesulfonamide are nanomolar-potent inhibitors of tumor-expressed carbonic anhydrase isozymes CA IX and CA XII. *Bioorganic Chemistry* **103**, 104204. https://doi.org/10.1016/j.bioorg.2020.104204
45. Wang, M., Qin, H-Li., Leng, J., Ameeduzzafar, , Amjad, M.W., Raja, M.A.G., Hussain, M.A., Bukhari, S.N.A., 2018. Synthesis and biological evaluation of new tetramethylpyrazine-based chalcone derivatives as potential anti-Alzheimer agents. *Chemical Biology & Drug Design* **92**, 1859-1866. https://doi.org/10.1111/cbdd.13355
46. Abdul Rahman, S., Bhatti, J., Thareja, S., Monga, V., 2023. Current development of 1,2,3-triazole derived potential antimalarial scaffolds: Structure- activity relationship (SAR) and bioactive compounds. *European Journal of Medicinal Chemistry* **259**, 115699. https://doi.org/10.1016/j.ejmech.2023.115699
47. Alalawy, A.I., Alatawi, K., Alenazi, N.A., Qarah, A.F., Alatawi, O.M., Alnoman, R.B., Alharbi, A., El-Metwaly, N.M., 2024. Synthesis, molecular modeling, and anticancer activity of new thiophene and thiophene-pyrazole analogues incorporating benzene-sulfonamide moiety as carbonic anhydrase isozymes (CA-IX and CA-XII). *Journal of Molecular Structure* **1295**, 136609. https://doi.org/10.1016/j.molstruc.2023.136609
48. Sajan, D., Joseph, L., Vijayan, N., Karabacak, M., 2011. Natural bond orbital analysis, electronic structure, non-linear properties and vibrational spectral analysis of L-histidinium bromide monohydrate: A density functional theory, *Spectrochimica Acta Part A: Molecular and Biomolecular Spectroscopy* **81**, 85-98. https://doi.org/10.1039/D0NJ05883A
49. Bulat, F.A., Chamorro, E., Fuentealba, P., Toro-Labbé, A., 2004. Condensation of frontier molecular orbital fukui functions. *The Journal of Physical Chemistry A* 108, 342-349. https://doi.org/10.1021/jp036416r
50. Xavier, S., Periandy, S., Ramalingam, S., 2015. NBO, conformational, NLO, HOMO-LUMO, NMR and electronic spectral study on 1-phenyl-1-propanol by quantum computational methods. *Spectrochimica Acta Part A: Molecular and Biomolecular Spectroscopy* **137**, 306-320. https://doi.org/10.1016/j.saa.2014.08.039
51. Makhlouf, M.M., Radwan, A.S., Ghazal, B., 2018. Experimental and DFT insights into molecular structure and optical properties of new chalcones as promising photosensitizers towards solar cell applications. *Applied Surface Science* **452**, 337-351. https://doi.org/10.1016/j.apsusc.2018.05.007
52. Bouchoucha, A., Zaater, S., Bouacida, S., Merazig, H., Djabbar, S., 2018. Synthesis and characterization of new complexes of nickel (II), palladium (II) and platinum(II) with derived sulfonamide ligand: Structure, DFT study, antibacterial and cytotoxicity activities. *Journal of Molecular Structure* **1161**, 345-355. https://doi.org/10.1016/j.molstruc.2018.02.057
53. Afolabi, S.O., Semire, B., Akiode, O.K., Idowu, M.A., 2022. Quantum study on the optoelectronic properties and chemical reactivity of phenoxazine-based organic photosensitizer for solar cell purposes. *Theoretical Chemistry Accounts* **141**. https://doi.org/10.1007/s00214-022-02882-w
54. Domingo, L., Ríos-Gutiérrez, M., Pérez, P., 2016. Applications of the conceptual density functional theory indices to organic chemistry reactivity. *Molecules* **21**, 748. https://doi.org/10.3390/molecules21060748
55. Bhagyasree, J.B., Varghese, H.T., Panicker, C.Y., Samuel, J., Van Alsenoy, C., Bolelli, K., Yildiz, I., Aki, E., 2013. Vibrational spectroscopic (FT-IR, FT-raman, 1H NMR and UV) investigations and computational study of 5-nitro-2-(4-nitrobenzyl) benzoxazole. *Spectrochimica Acta Part A: Molecular and Biomolecular Spectroscopy* 102, 99-113. https://doi.org/10.1016/j.saa.2012.09.032
56. Olasunkanmi, L.O., Obot, I.B., Ebenso, E.E., 2016. Adsorption and corrosion inhibition properties of n-{n-[1-r-5-(quinoxalin-6-yl)-4,5-dihydropyrazol-3-yl] phenyl}methanesulfonamides on mild steel in 1 M HCl: Experimental and theoretical studies. *RSC Advances* **6**, 86782-86797. https://doi.org/10.1039/c6ra11373g
57. El Adnani, Z., Mcharfi, M., Sfaira, M., Benzakour, M., Benjelloun, A.T., Ebn Touhami, M., 2013. DFT theoretical study of 7-r-3methylquinoxalin-2(1H)-thiones (RH; CH3; cl) as corrosion inhibitors in hydrochloric acid. *Corrosion Science* **68**, 223-230. https://doi.org/10.1016/j.corsci.2012.11.020
58. Mi, H., Xiao, G., Chen, X., 2015. Theoretical evaluation of corrosion inhibition performance of three antipyrine compounds. *Computational Theoretical Chemistry* **1072**, 7-14. https://doi.org/10.1016/j.comptc.2015.08.023
59. Messali, M., Larouj, M., Lgaz, H., Rezki, N., Al-Blewi, F.F., Aouad, M.R., Chaouiki, A., Salghi, R., Chung, I.-M., 2018. A new schiff base derivative as an effective corrosion inhibitor for mild steel in acidic media: Experimental and computer simulations studies. *Journal of Molecular Structure* **1168**, 39-48. https://doi.org/10.1016/j.molstruc.2018.05.018
60. Roy, R.K., Krishnamurti, S., Geerlings, P., Pal, S., 1998. Local softness and hardness based reactivity descriptors for predicting intra- and intermolecular reactivity sequences: Carbonyl compounds. *The Journal of Physical Chemistry A* **102**, 3746-3755. https://doi.org/10.1021/jp973450v
61. Roy, R., F.d. de Proft, P. 1998. Geerlings, Site of protonation in aniline and substituted anilines in the gas phase: a study via the local hard and soft acids and bases concept. *The Journal of physical chemistry A* **102**, 7035-7040.
62. Roy, R.K., Pal, S., Hirao, K., 1999. On non-negativity of fukui function indices. J. Chem. Phys. 110, 8236-8245. https://doi.org/10.1063/1.478792
63. Sun, Y., Chen, X., Sun, L., Guo, X., Lu, W., 2003. Nanoring structure and optical properties of Ga8As8. *Chemical Physics Letters* **381**, 397-403. https://doi.org/10.1016/j.cplett.2003.09.115
64. Abraham, J., Sajan, D., Joe, I., Jayakumar, V., 2008. Molecular structure, spectroscopic studies and first-order molecular hyperpolarizabilities of p-amino acetanilide. *Spectrochimica Acta Part A: Molecular and Biomolecular Spectroscopy* **71**, 355-367. https://doi.org/10.1016/j.saa.2008.01.010
65. Karamanis, P., Pouchan, C., Maroulis, G., 2008. Structure, stability, dipole polarizability and differential polarizability in small gallium arsenide clusters from all-electron ab initio and density-functional-theory calculations, *Physical Review A: Atomic, Molecular, and Optical Physics* **77**, 013201. https://doi.org/10.1103/PhysRevA.77.013201
66. Aziz, M., Ejaz, S., Tamam, N., Siddique, F., Riaz, N., Qais, F., Chtita, S., Iqbal, J., 2022. Identification of potent inhibitors of NEK7 protein using a comprehensive computational approach. *Scientific Reports* **12**, 6404. https://doi.org/10.1038/s41598-022-10253-5
67. Ahmed, A.B., Feki, H., Abid, Y., Boughzala, H., Mlayah, A., 2008. Structural, vibrational and theoretical studies of l-histidine bromide. *Journal of Molecular Structure* **888**, 180-186. https://doi.org/10.1016/j.molstruc.2007.11.056